Received: 4 April 2020 | Revised: 25 April 2020 | Accepted: 5 May 2020

DOI: 10.1002/eom2.12027

EcoMat FUNCTIONAL MATERIALS FOR GREEN ENERGY AND ENVIRONMENT WILEY

REVIEW

# Antimony-based nanomaterials for high-performance potassium-ion batteries

**Hong Gao**[1] | **Xin Guo**[2] | **Shijian Wang**[2] | **Fan Zhang**[2] | **Hao Liu**[2] | **Guoxiu Wang**[2]

[1]Joint International Laboratory on Environmental and Energy Frontier Materials, School of Environmental and Chemical Engineering, Shanghai University, Shanghai, China

[2]Centre for Clean Energy Technology, School of Mathematics and Physics, Faculty of Science, University of Technology Sydney, Sydney, New South Wales, Australia

**Correspondence**
Xin Guo, Hao Liu and Guoxiu Wang, Centre for Clean Energy Technology, School of Mathematics and Physics, Faculty of Science, University of Technology Sydney, Broadway, Sydney, NSW, Australia.
Email: xin.guo@uts.edu.au, hao.liu@uts.edu.au, guoxiu.wang@uts.edu.au

**Funding information**
Australian Research Council, Grant/Award Numbers: DP180102297, IH180100020; China Postdoctoral Science Foundation, Grant/Award Number: 2019M661464

## Abstract

Potassium-ion batteries (PIBs) present great potential for large-scale energy storage applications owing to their high energy density and the abundance of potassium reserve. However, the large radius of $K^+$ and super-reactive metallic nature of potassium make it difficult to realize electrochemically reversible storage with most conventional electrode materials. Currently, it remains a great challenge to develop appropriate anode materials with high specific capacities, long cycle life, and low cost for PIBs. Antimony-based materials are recognized as a promising anode candidate because of their high theoretical capacities, appropriate potassiation potential, and relatively low cost. Herein, we review the recent progress of antimony-based anode materials for PIBs, including metallic antimony, antimony-based alloys, antimony chalcogenides, and composite combinations. Meanwhile, this review also focuses on the electrochemical reaction mechanisms, strategies for design and synthesis of electrode materials, and the advances of electrolyte modulation and electrode formulation. Finally, we present the critical challenges to be addressed and perspectives for ways forward to promote the development of PIBs.

**KEYWORDS**

antimony chalcogenides, conversion and alloying mechanisms, electrolytes modulation, materials nanoengineering, potassium-ion batteries, Sb-based anodes

## 1 | INTRODUCTION

The fast-growing demands of electric vehicles (EVs) and smart grids are stimulating the development of energy storage systems with low cost and high energy density. Although the state-of-the-art lithium-ion batteries (LIBs) will probably continue to play an important role in EVs, portable electronic, and large-scale energy storage, it is imperative to explore alternative battery systems due to the limited and regional lithium resources.[1-3] Potassium-ion batteries (PIBs) are regarded as a potential alternative to LIBs, particularly in large-scale energy storage applications because of the abundance of potassium resources and its similar chemistry to lithium. Moreover, the standard reduction potential of potassium (−2.93 V vs $E_0$) endows PIBs a high-voltage output, which is expected to advantageously compensate for the heavier atomic mass compared to Li. Besides, the lower charge density of $K^+$ leads to smaller solvated ions and weaker desolvation

energy of potassium, thereby offering higher ionic conductivity in the bulk electrolyte.[4-7]

The large ionic radius of $K^+$ (1.38 Å) results in significant challenges to develop high-performance electrode materials, which can tolerate the structural changes during repeated intercalation/deintercalation process and simultaneously achieve fast kinetics and satisfactory cycling stability.[8-11] Furthermore, metallic potassium cannot be directly employed as an anode due to the safety concerns stemming from its violent reactivity.[12,13] Although some researchers have demonstrated that the commercial graphite anodes used in LIBs can achieve an improved cycling performance with optimized electrolytes in PIBs, the obtained capacity is still limited, and graphite anode also suffer from large volume expansion during $K^+$ intercalation.[14-16] Therefore, many research efforts have been devoted to exploring suitable anode materials. These include carbonaceous materials,[17-20] metal oxides,[21,22] transition-metal carbides and chalcogenides,[23-26] metal alloys,,[27-30] and their composites.[31,32]

Among these candidates, metallic antimony (Sb) and Sb-based materials stand out owing to their high theoretical capacities and low working potential.[33] As shown in Figure 1A, metallic Sb can deliver a capacity of 660 mAh $g^{-1}$ with the formation of $K_3Sb$ alloy upon fully potassiation, which is much higher than those of graphitic carbon and other alloy-based anodes except for phosphorus (P). However, compared to the P, the Sb-based anodes are advantageous in term of electronic conductivity and easiness for fabricating nanostructured electrodes, both of which are essential to facilitating the sluggish electrochemical kinetics in PIBs. Meanwhile, the puckered-layer structure of Sb with a low stacking density is beneficial for ionic diffusion and release of structural strain.[34] Thus, the electrochemical reaction kinetics of the PIBs could be boosted, leading to small polarization and good rate capability. The small polarization between charge and discharge can lead to a high round trip-efficiency of the battery. Consequently, the safety risks of self-heating inside the cells can be mitigated.[35] Furthermore, the relative low discharge plateau of the Sb-based anodes would improve the energy density of practical PIBs.

However, the huge volumetric expansion (~400%) of Sb-based anodes deriving from the formation of $K_3Sb$ alloy after fully potassiation creates gigantic inner stresses in the electrode, which leads to the pulverization of the active material and loss of electrical contact between electrode material and current collector, resulting in the rapid capacity decay. These issues are similar to the ones that Si-based anodes and other alloy-type materials faced in LIBs.[36,37] Thus, the experience accumulated in those fields can be potentially employed for the improvement of Sb-based materials in PIBs. For example, improved performances can be achieved by downsizing bulk Sb into nanoparticles, combining nanosized Sb with different carbon matrices, and applying a multitude of strategies to delicately construct the Sb-containing porous architectures and nanocomposites.[38-40] Furthermore, transforming Sb into Sb-based bimetallic alloys or antimony oxides/sulfides/selenides could be another approach to alleviate the pulverization problem and stabilize the cycling performance.[41] These rationally designed strategies can effectively retard volume expansion, accelerate ions and electron transport, and eventually improve the cycling stability and rate capability of Sb-based electrodes.[42-44] In addition, the optimization of electrolytes and parameters for electrode formulation can also improve potassium storage capability of the Sb-base anode materials.

Herein, we summarize the recent advances of Sb-based anode materials for PIBs, including pure Sb and its composites, Sb-based alloys, and relevant antimony oxides, sulfides or selenides (Figure 1B). To give a balanced and detailed overview of this field, we have systematically reviewed the understanding of relevant reaction mechanisms, rational electrode structural engineering strategies, and impacts of the electrolyte and electrode formulations on electrochemical performances. Moreover, we also highlight the existing

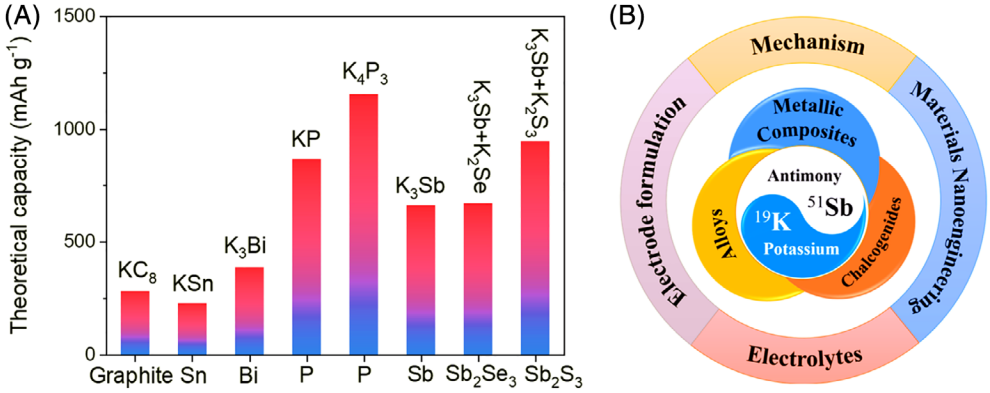


**FIGURE 1** A, The theoretical capacity and corresponding discharge products of the mostly studied alloy-based materials for potassium storage (graphite is presented as reference). B, Schematic illustration of the methodology for improving electrochemical performance of Sb-based anodes in potassium-ion batteries

challenges and opportunities for preparing high-performance Sb-based anodes materials for PIBs. We believe that this review is instructive and informative for researchers working on the development of new rechargeable battery systems.

## 2 | MONOMETALLIC Sb-BASED ANODES

### 2.1 | Potassium storage mechanism of metallic Sb anodes

Understanding the working mechanism and identifying the exact discharge and charge products during each potassiation/depotassiation step is crucial to guiding electrode design and determining appropriate methods to enhance the electrochemical performances of Sb-based anode materials in PIBs. Although metallic Sb possesses a high theoretical capacity of 660 mAh $g^{-1}$ (same as the capacities for lithium and sodium storage) upon full alloying by the formation of $K_3Sb$ in PIBs, the mechanism of potassium storage is different from those in LIBs and sodium-ion batteries (SIBs).[45-47]

So far, several different characterization methods have been employed for unraveling the potassium storage mechanism in Sb-based anodes, including ex situ and in situ X-ray diffraction (XRD), ex situ Raman spectroscopy, and transmission electron microscopy (TEM). McCulloch et al firstly reported a mechanically mixed Sb/C nanocomposite for PIBs in 2015. This anode material delivered an initial reversible capacity of ~650 mAh $g^{-1}$ (98% of the theoretical capacity of Sb), indicating that the Sb/C hybrid can alloy with potassium forming a $K_3Sb$ alloy.[38] The discharge product was further confirmed by ex situ XRD, in which the diffraction peaks of the pristine and fully discharged electrodes match those of pure crystalline antimony and cubic $K_3Sb$ phase, respectively. Compared with the ex situ XRD techniques, in situ characterization is more powerful for accurately monitoring the phase changes during discharging and charging processes. For example, Mai et al revealed the K-Sb alloying

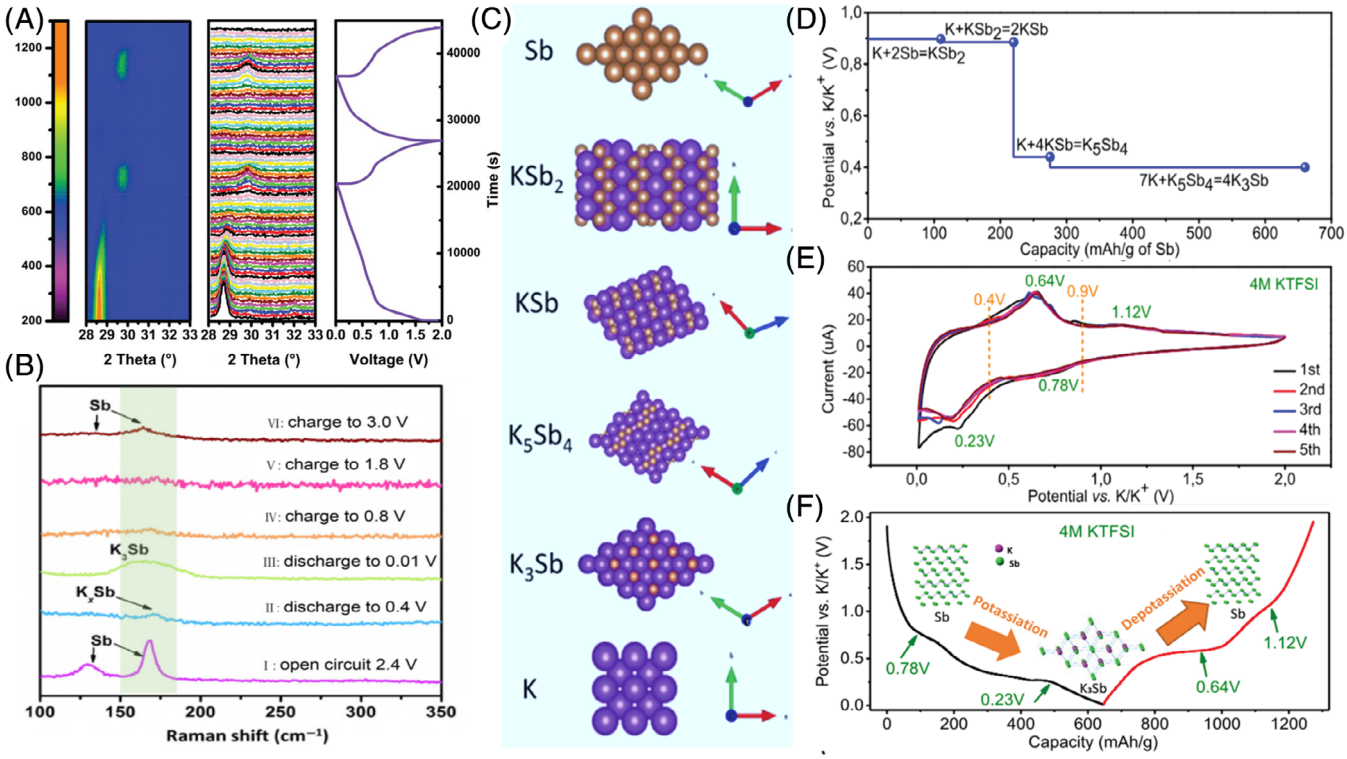


**FIGURE 2** A, In situ X-ray diffraction patterns of the three-dimensional SbNPs@C electrode during the galvanostaticde potassiation/depotassiation process at 100 mA $g^{-1}$, image plot of the diffraction patterns at 28° to 33° during the first two cycles. Reproduced with permission from Reference 48, Copyright 2017, Royal Society of Chemistry. B, Ex situ Raman spectra of a Sb/C electrode collected at different states at a current density of 0.5 A $g^{-1}$. Reproduced with permission from Reference 49, Copyright 2019, Springer. C, Crystal structure of K and stages of the structure evolution from Sb to $K_3Sb$ during the potassiation process. D, Density functional theory-calculated equilibrium voltages (vs $K/K^+$) for the potassiation process. E, Cyclic voltammetry curves for the Sb@CSN electrode at a scan rate of 0.05 mV $s^{-1}$. F, Typical second charge/discharge profile Sb@CSN in the 4 M potassium trifluoromethane-sulfonimide (KTFSI) electrolyte at 50 mA $g^{-1}$. Reproduced with permission from Reference 50, Copyright 2019, Royal Society of Chemistry

reaction in a three-dimensional (3D) confined Sb nanoparticles (SbNPs@C) anodes by in situ XRD measurements.[48] As shown in Figure 2A, the diffraction peak of Sb at 28.6° was clearly detected in the pristine electrode, and this peak gradually disappeared upon discharging and a new peak of $K_3Sb$ located at 29.7 ° appeared when discharged to 0.19 V. No diffraction peaks were detected between 28.6° and 29.7 °, indicating that the intermediate discharge products are amorphous.[51] Upon charging, the peak intensity of $K_3Sb$ gradually decreases, and amorphous Sb was obtained as the final product, which was further confirmed by ex situ TEM. In addition, ex situ Raman spectroscopy has been employed as another useful technique to verify the potassiation mechanism of Sb anodes (Figure 2B).[49]

Beyond the aforementioned direct characterization methods to investigate the structure of discharge products, theoretical calculations were also conducted to predict the potassiation behavior of Sb anodes. According to the Sb-K binary phase diagram, there are four $K_xSb$ intermediate phases ranging from $KSb_2$ to KSb, $K_5Sb_4$, and $K_3Sb$ along with the increase of K content (the crystalline structures are shown in Figure 2C), corresponding to theoretical capacities of 108, 216, 270, and 660 mAh $g^{-1}$ in PIBs, respectively.[52] On the basis of the phase diagram, Wang et al computed the equilibrium potential for alloying K with Sb via first principle calculations.[50] As exhibited in Figure 2D, the thermodynamic equilibrium potentials of $KSb_2$, KSb, $K_5Sb_4$, and $K_3Sb$ are 0.89, 0.849, 0.439, and 0.398 V, respectively. The calculated two prominent potential plateaus at voltages of ~0.4 and 0.9 V are in accordance with two redox peaks observed in the cyclic voltammetry (CV) curves (Figure 2E). The broad overlapping peak located at ~0.78 V in the cathodic scan could be attributed to the formation of intermediates $KSb_2$/KSb. Meanwhile, another overlap peak centered at ~0.23 V should be assigned to the stepwise alloying reactions from KSb to $K_5Sb_4$ and then $K_3Sb$. In the reverse anodic curve, a prominent peak at 0.64 V and a minor peak at 1.12 V, correspond to the stepwise K extraction from $K_3Sb$ to Sb. It should be noted that the peaks are shifted in the CV curves compared with the theoretical value, which is primarily due to the overall system overpotential. Figure 2F shows the second galvanostatic charge/discharge curves of the as-prepared Sb-C composite in 4 M potassium trifluoromethane-sulfonimide (KTFSI) electrolyte at 50 mA $g^{-1}$. It is obvious that the voltage plateaus and intensity of discharging/charging curves are consistent with the CV results and calculated voltage profile.

Overall, advanced in situ and ex situ characterizations play crucial roles in investigating the detailed working mechanisms of PIBs. A better understanding of the electrochemical behaviors provides us a deep insight for developing Sb-based anodes, or even other alloying-type electrode materials for PIBs.

## 2.2 | Modification strategies for Sb-based anodes

Similar to most other alloying-type anode materials, Sb suffers from significant volume changes during repeated potassiation/depotassiation processes, which leads to pulverization of the electrode material and fracture of the active material from the current collector, manifesting as abrupt capacity fading. To overcome these challenges, several strategies have been reported. These include engineering nanostructures to shorten $K^+$ diffusion pathways and accommodate the volume extension, incorporating a complementary matrix to buffer the structural changes, and optimizing electrolytes composition to mitigate the side reactions and stabilize the solid electrolyte interface (SEI).

### 2.2.1 | Nanostructured Sb

Nanostructuring is becoming a key technique for improving electrochemical performances of electrode materials since it can enhance the reaction kinetics by shortening the pathways for electron transport and ion diffusion. Meanwhile, the voids between nanomaterials or within nanoarchitectures can alleviate the mechanical stress caused by the volume changes of active materials compared with the bulk counterparts (Figure 3A). Qian et al synthesized Sb nanoparticles with an average size of 55 nm by a low-temperature molten salt reduction of $SbCl_3$ (Figure 3B).[53] As shown in Figure 3C, the Sb nanoparticles exhibit a better rate performance compared with the bulk one, indicating the enhanced electrochemical reaction kinetics of nanosized Sb electrodes due to the shorter diffusion distance and reduced mechanical stress. Although some improvements in performance has been achieved from bulk to nanosized material, the capacity of Sb nanoparticles suddenly drops to less than 100 mAh $g^{-1}$ after 20 cycles. The reason for this failure is that the electrode has no ample space to accommodate the volume expansion of the Sb during potassiation. Therefore, design and construction of nanoarchitectures with void space and pores could further improve electrochemical performance.[55,56]

As an example, Feng et al prepared a micronsized nanoporous Sb with tunable porosity by a vacuum distillation strategy for high-performance PIBs.[54] The nanoporous Sb was obtained through evaporating low-boiling-point Zn from a commercial Zn-Sb alloy

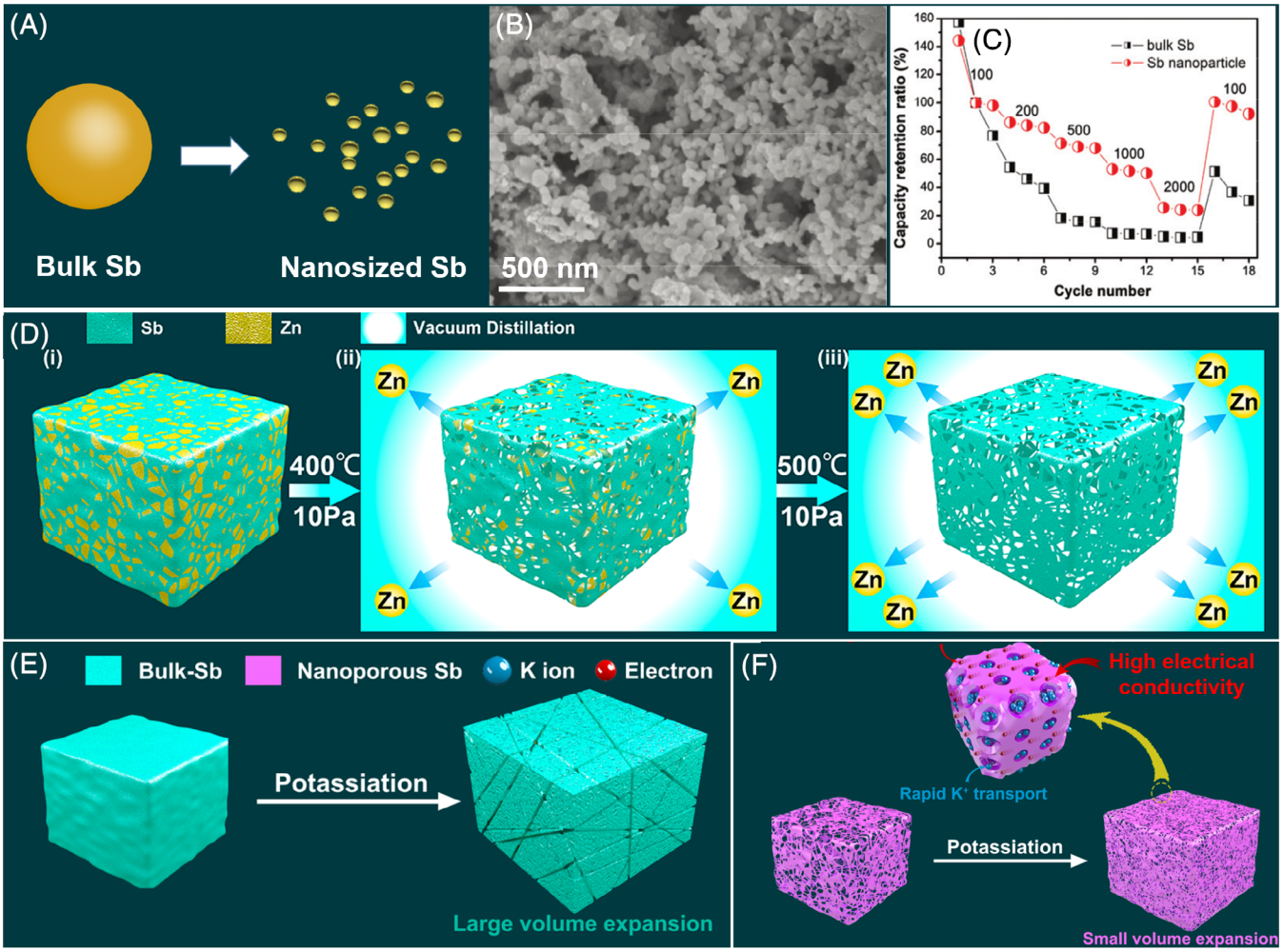


**FIGURE 3** A, Schematic of the reducing grain size of bulk Sb material to the nanoscale. B, Scanning electron microscopy image of Sb nanoparticles. C, A comparison of rate performances of the bulk Sb and Sb nanoparticles. Reproduced with permission from Reference 53, Copyright 2018, Royal Society of Chemistry. D, Schematic of the preparation of nanoporous Sb by the vacuum-distillation approach. Schematic of potassiation process for the, E, bulk Sb and, F, nanoporous Sb anodes. Reproduced with permission from Reference 54, Copyright 2018, American Chemical Society

(Figure 3D). Meanwhile, the pore volume of 3D nanoporous Sb can be controlled by adjusting the evaporation temperature and the proportion of Zn-Sb. The pure nanoporous Sb electrode delivered an initial charge capacity of 517 mAh $g^{-1}$ with a capacity retention of 62.35% after 50 cycles at 50 mA $g^{-1}$ and rate capacity of 265 at 500 mA $g^{-1}$. By contrast, the bulk Sb only retained 3.92% of the original capacity after 50 cycles. The poor cycling performance of the bulk-Sb could be attributed to the crumbling of the conductive network between Sb particles and current collector due to the large volume expansion upon potassiation (Figure 3E). In contrast, the micron-sized Sb with interconnected nanopores is beneficial to accommodate the volume change and promote electron and ion transport during the alloying-dealloying processes (Figure 3F). Even with these advantages, the cycling stability of pure 3D porous Sb is still not as good as that of carbon materials since the whole Sb skeleton is vulnerable to the mechanical stress caused by the repeated insertion and extraction of $K^+$ ions.[57]

### 2.2.2 | Hybridization of nanostructured Sb and conductive matrixes

Combining Sb nanoparticles and conductive matrixes can further stabilize the electrode structures and improve the cycling performance of PIBs. Mechanical blending methods, such as hand grinding, ball milling, and ultrasonic treatment, are one of the most simple and efficient approach to achieve the hybridization of Sb nanoparticle and carbonaceous materials.[58] High-energy ball milling and high-power ultrasonication can also downsize multiple composite particles simultaneously.[59] The carbon

ratio in the Sb/C composite is crucial to electrochemical performance as well. Sultana et al demonstrated that a higher carbon proportion in the composite could postpone battery failure in a later cycle, but the capacity of the composite electrode would become lower when more carbon was incorporated.[60] In addition, extended milling and ultrasonic treatment time lead to a smaller Sb particle size and more uniform distribution of particles on a supporting substrate, thereby improving electrochemical performance. For example, Lu et al prepared Sb-graphite composites via 24 hours high energy ball-milling along with an ultrasonic method, in which Sb nanoclusters of less than 5 nm size uniformly distributed in the graphite layers.[61] The Sb-graphite hybrid anode delivered a reversible capacity of 449.7 mAh $g^{-1}$ after 100 cycles with a capacity retention of 96.8%, which is much higher than that of Sb-graphite prepared by hand grinding. Nevertheless, the battery life of most mechanically mixed Sb/C composites is under 100 cycles and an abrupt drop in capacity occurs in the later cycles. This is because the mechanical mixing method inevitably leads to an uneven distribution of the Sb and carbon, and still no ample reserved space for accommodating the volume expansion of Sb and releasing the accompanying mechanical stress of the whole structure.

The structural stability of Sb-anodes can be further enhanced by anchoring Sb nanoparticles on a variety of conductive nanomaterial matrixes, such as one-

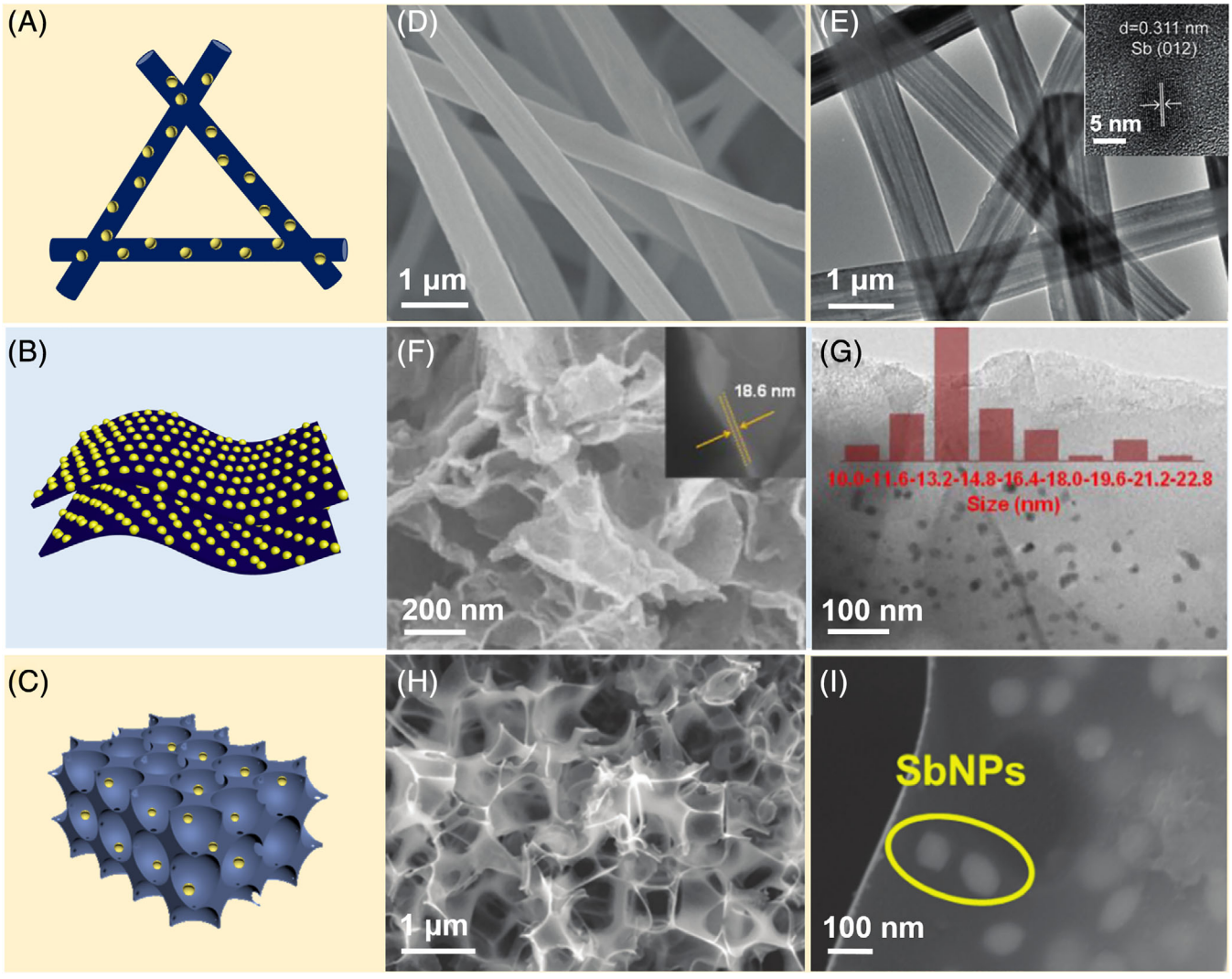


**FIGURE 4** Schematic illustrations of the Sb nanoparticles anchored on the, A, one-dimensional (1D) nanofibers, B, two-dimensional (2D) nanosheets, and, C, three-dimensional (3D) porous network. D, Scanning electron microscopy (SEM) and, E, transmission electron microscopy (TEM) images of the u-Sb@CNFs. Reproduced with permission from Reference 64, Copyright 2019, Wiley-VCH. F, SEM image, G, TEM image and (inset of G) particle size distribution of the Sb/CNS. Reproduced with permission from Reference 66, Copyright 2019, Elsevier. H, Low-magnification and, I, high-magnification SEM images of 3D SbNPs@C. Reproduced with permission from Reference 48, Copyright 2018, Royal Society of Chemistry

dimensional (1D) nanotubes or nanofibers,[62-64] two-dimensional (2D) nanosheets,[65] and 3D networks (Figure 4A-C).[67] 1D materials not only act as highly conductive continuous networks but also provide high mechanical strength. Meanwhile, 1D structures are readily interwoven into flexible free-standing electrodes, which is attractive for wearable devices. More importantly, the empty spaces between the 1D structures facilitate electrolyte penetration and accommodate volume changes of Sb particles, enabling better cycling stability.[68] For instance, Zhou et al fabricated the ultrasmall Sb nanoparticles within carbon nanofibers containing an array of hollow nanochannels (u-Sb@CNFs) via a hard-template assisted electrospinning technique (Figure 4D-E).[64] When employed as free-standing anodes for PIBs, they achieved an excellent rate capability and superior cycling stability (retaining a capacity of 225 mAh $g^{-1}$ after 2000 cycles at 1 A $g^{-1}$).

Owing to the advantages of shorter ion diffusion pathways, larger surface-to-volume ratio and higher utilization of active sites, 2D materials have attracted intensive attention for energy storage.[69-71] However, the severe restacking tendency of 2D nanosheets hinders the access of electrolyte and ionic transport.[72] Combining Sb nanoparticles with conductive 2D materials, such as graphene and MXenes, can utilize the advantages of both individual components and eliminate their shortcomings.[73] The 2D materials not only provide fast electronic and ionic pathways for electrochemical reactions, but also protect Sb from the pulverization. Meanwhile, Sb nanoparticles act as pillars to prevent the restacking of the 2D materials. As shown in Figure 4F,G, Sb nanocrystals with a size of ~14.0 nm embedded into ultrathin carbon nanosheets (Sb/CNS) were prepared by a solvothermal "metathesis" reaction.[66] Owing to the synergistic effects between carbon nanosheets and Sb nanoparticles, the Sb/CNS electrode delivered a specific capacity of 288 mAh $g^{-1}$ at 50 mA $g^{-1}$ after 50 cycles and maintained 90% of the initial capacity after 600 cycles at 200 mA $g^{-1}$.

Similar to 1D structures, another advantage of 2D materials is the possibility of forming flexible electrodes without binders and additives. Recently, 2D transition metal carbides and/or nitrides, denoted as MXenes, have been widely applied as electrode materials or complementary additives in energy storage due to their high electronic conductivity and low ion diffusion barriers.[74-76] Based on these merits of 2D MXenes, Tian et al constructed a robust, flexible and free-standing MXene@Sb anode via a one-step electrodeposition approach.[77] Hierarchically porous Sb was robustly grown on the MXene paper, which provided high efficient pathways for the migration of electrons and ions. The MXene@Sb anode showed a reversible capacity of 517 mAh $g^{-1}$ at 500 mA $g^{-1}$ with ~79.1% capacity retention after 500 cycles in PIBs. After 100 cycles, the MXene@Sb electrode maintained integrity and flexibility. In particular, the porous Sb particles were well preserved, demonstrating the good structural stability of the composite. In addition, the free-standing electrode without using Al or Cu current collectors could decrease the weight of batteries and thus increase the energy density of full cells.

Owning to the high surface area, continuously interconnected networks and superior conductivity, 3D porous carbonaceous architectures are generally considered as ideal buffer frameworks to relieve structural fracture of Sb, enhance ionic and electronic transport, and maintain electrode integrity.[78,79] As shown in Figure 4H,I, Han et al constructed Sb nanoparticles (~100 nm) confined in a honeycomb-like carbon network (SbNPs@C) by a NaCl template method for potassium storage.[48] The as-prepared SbNPs@C anodes possessed the advantages of the 3D carbon framework and the high capacity of the Sb, and exhibited a good rate performance with a capacity of 288 mAh $g^{-1}$ at a high current density of 1 A $g^{-1}$. Similarly, Chen et al prepared a 3D macroporous Sb-carbon composite (Sb@C-3DP) through a facile KCl template strategy coupled with a bi-functional potassium antimony tartrate as precursor.[67] The Sb@C-3DP electrodes maintained an outstanding capacity of 342 mAh $g^{-1}$ with a retention of 97% at 0.5 A $g^{-1}$ after a long life span of 260 cycles. Moreover, the full cells consisting of Sb@C-3DP anodes and the Prussian blue cathodes exhibited a high energy density (197.6 Wh $kg^{-1}$) and power density (2067.9 W $kg^{-1}$) in potassium bis(fluorosulfonyl)imide-dimethoxyethane (KFSI-DME) electrolyte.

Beyond the above three kinds of typical nanocomposites, there have several other Sb-based hybrid structures been reported. For example, Kim et al and Lu et al both reported a multicomposite electrode (Sb-C-rGO) comprising Sb nanoparticles, amorphous carbon and graphene sheets, in which Sb was confined in the carbon matrix, and the reduced graphene oxide acted as extra reinforcement for conductive and mechanical properties.[80,81] Because of these advantages, the pulverization of active material was circumvented, and the robust Sb-C-rGO composite electrodes achieved a significantly improved rate performance and excellent cycling stability (Figure 5A). Besides these features, the capacity of the Sb-C-rGO anode recovered to the original value after 100 cycles after replacing the K metal and electrolyte, demonstrating that the degradation of the batteries was mainly due to the side reactions between the carbonate electrolyte and K metal (Figure 5B). The result also suggests the necessity of developing alternative anodes instead of using metallic K as anodes.

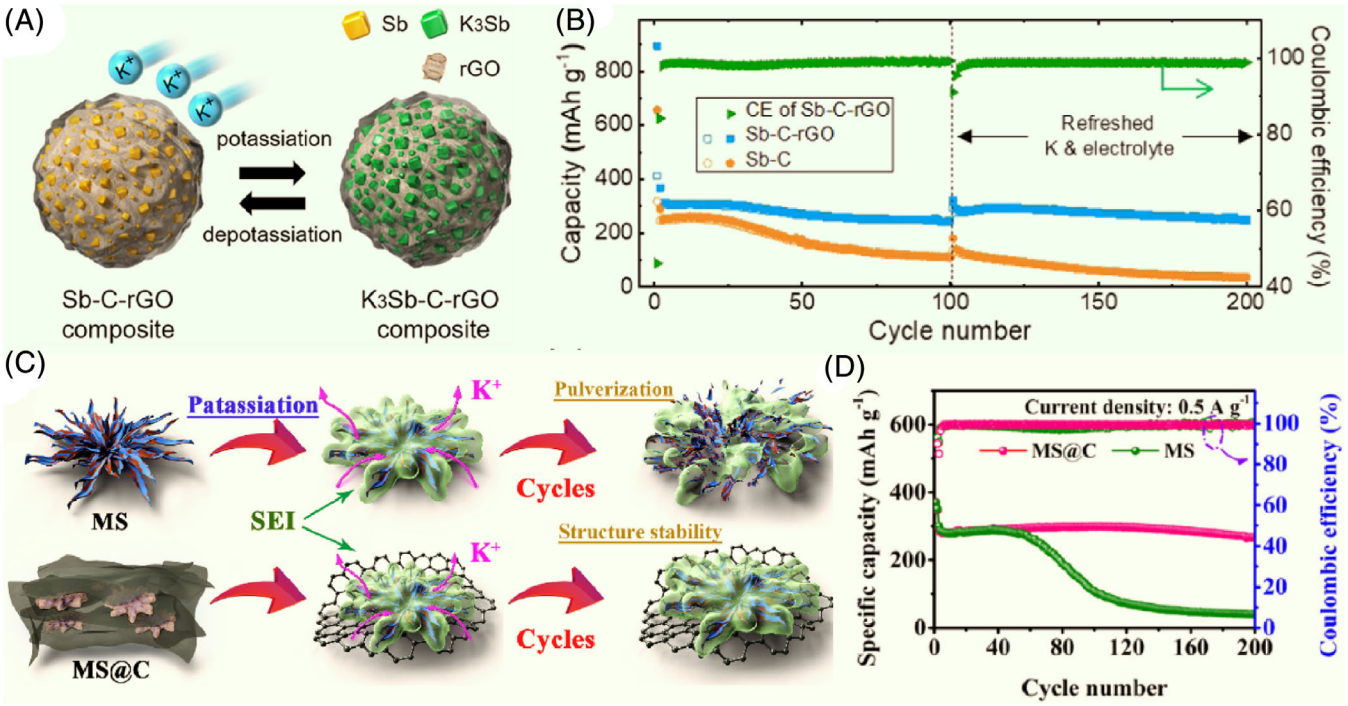


**FIGURE 5** A, Schematic of the structural evolution of the Sb-C-rGO during potassiation and depotassiation. B, Cycling performance of the Sb-C and Sb-C-rGO composites at 0.5 A $g^{-1}$. Reproduced with permission from Reference 81, Copyright 2019, American Chemical Society. C, Schematic illustration of the MS@C and $MoS_2$/Sb heterostructure (MS) composites during long-term cycling. D, Cycling performance of the MS@C and MS at 0.5 A $g^{-1}$. Reproduced with permission from Reference 82, Copyright 2019, Elsevier

Qu et al introduced a hierarchical chrysanthemum-like $MoS_2$/Sb heterostructure (MS) encapsulated into an N-doped graphene framework (MS@C) for PIBs.[82] Firstly, the MS with Sb nanoparticles uniformly distributed on the $MoS_2$ nanosheets provided more active sites for potassium storage since the open chrysanthemum-like structure provide enormous contact areas between the electrolyte and active material (Figure 5C). Moreover, $MoS_2$ also contributed a significant capacity based on the conversion reaction. Secondly, the heterointerfaces formed between $MoS_2$ nanosheets and Sb nanoparticles confined the coarsening of Sb nanocrystals and mitigated structural collapse during potassiation and depotassiation. Thirdly, the N-doped graphene framework further facilitated electron transport and enhanced structural stability by preventing the agglomeration and pulverization of $MoS_2$ and Sb. Thus, the MS@C electrode delivered better cycling stability than that of MS (Figure 5D).

## 3 | Sb-BASED ALLOYS FOR PIBs

Combining Sb with another metal to form intermetallic alloys is considered as an effective approach to alleviate the volume expansion of Sb anode and improve its electrochemical performance.[83] Based on the chemical reactivity of the introduced metal, the Sb-based alloys can be divided into the active-inactive and active-active types. Both types can reduce the aggregation of Sb nanoparticles and buffer the volume changes of Sb or Sb and the other active metal during potassiation and depotassiation. It should be noted that the alloys alone, especially for the active-active type, mostly still suffer from the electrochemical pulverization and limited cycle life, and the aforementioned strategies for modification of metallic Sb are suitable for further improving their performances. For active-inactive alloys, such as Sb-Co and Sb-Fe alloys, the introduction of the inactive conductive metal could enhance the rate capability and cycling stability of Sb, but at the cost of specific capacity of the whole electrode.[84,85]

On the other hand, the active-active type alloys are more promising since both components contribute to the capacity of potassium storage, leading to a higher specific capacity. Recently, Xu et al constructed a bismuth-antimony/carbon composite (BiSb@C) by a freeze-drying and pyrolysis method (Figure 6A).[86] Bi was chosen because it could form solid solutions with Sb at any molar ratios, and it also has a reasonable theoretical capacity of 385 mAh $g^{-1}$ for potassium storage. The XRD, scanning electron microscopy (SEM), and TEM characterization results revealed BiSb alloy nanoparticles

uniformly embedded in porous carbon nanosheets (Figure 6B-E). Due to the synergistic effects between the Bi, Sb, and carbon, the BiSb@C anodes delivered a higher capacity and better cycling stability compared with the monometallic counterparts (Figure 6F). The excellent performance could be attributed to the highly reversible electrochemical alloying and dealloying reaction, which was revealed by the operando XRD characterization (Figure 6G). Generally, the potassiation and depotassiation processes are similar to metallic Sb, except that a crystalline BiSb phase was observed instead of the amorphous Sb when batteries were fully charged.

Tin-antimony (SnSb) is another extensively investigated bimetallic alloy for PIBs. Sn has a very limited specific capacity (226 mAh $g^{-1}$) based on the formation of KSn after potassiation. However, Sn has a much lower discharge plateau which is favorable for anodes. When Sn alloying with Sb, the attainable capacity can be increased compared with the bare Sn anode. More importantly, the SnSb alloy possesses different alloying/dealloying potentials of the Sn and Sb, and the synergistic effects between Sb and Sn can alleviate the dramatic volume variation during discharge and charge.[87] As a demonstration, Stievano et al prepared SnSb powder via a high energy ball milling method.[41] The alloy anode achieved a specific capacity of 370 mAh $g^{-1}$ with a 75% capacity retention after 40 cycles based on the formation of KSn and $K_3Sb$ after potassiation, and the cycling stability is better than that of pure Sn and Sb electrodes. Undoubtedly, pure SnSb with delicately designed nanostructure and carbon modification can further facilitate K diffusion kinetics and prevent the aggregation of nanoalloy particles. Zhao et al fabricated SnSb nanoparticles confined in N-doped 3D carbon composite (SnSb@NC) through a NaCl template-assisted in situ pyrolysis method for PIBs.[88] The porous N-doped carbon

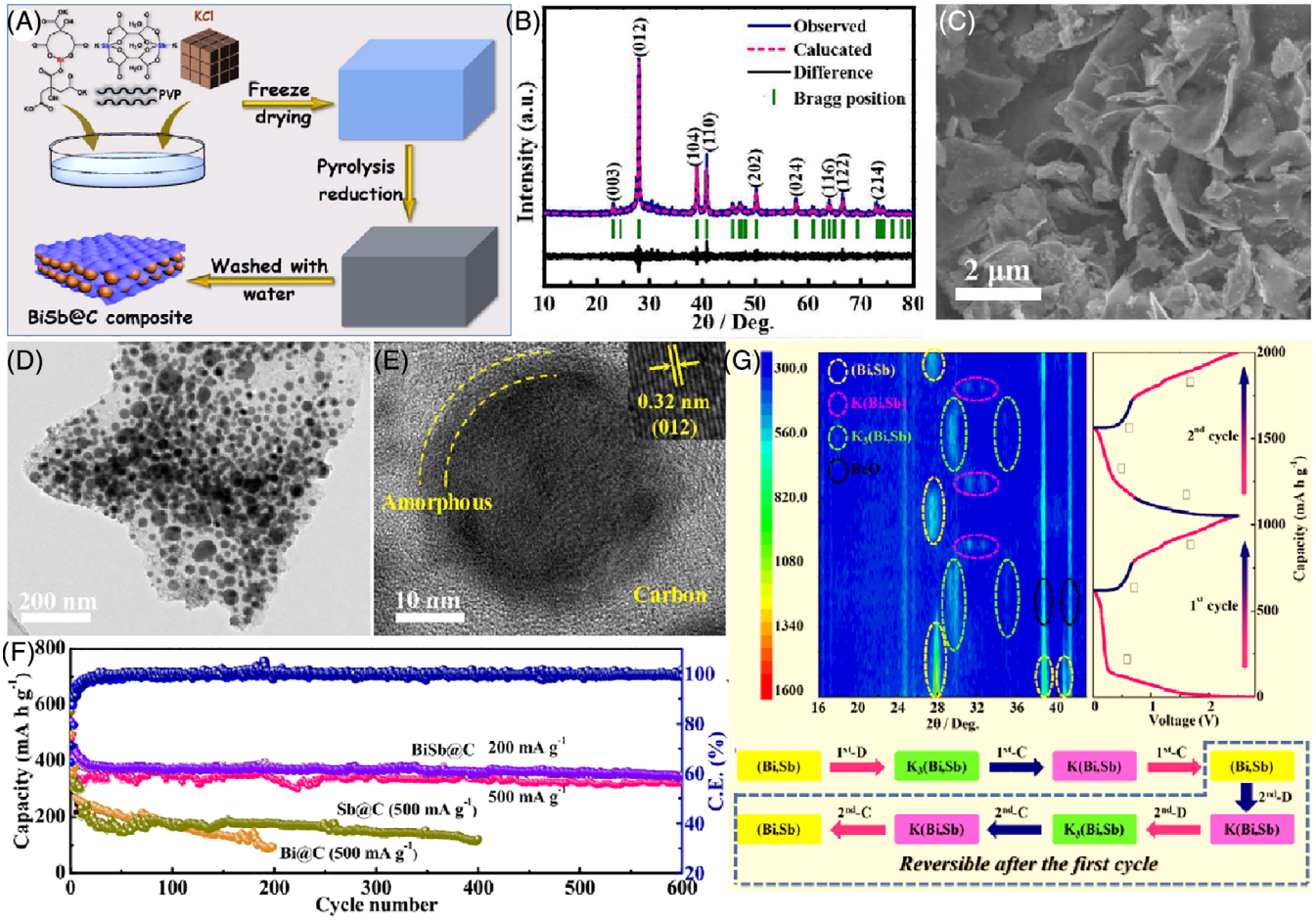


**FIGURE 6** A, Schematic illustration of the preparation of the BiSb@C composite. B, X-ray diffraction (XRD) pattern with Reitveld-refined results, C, Scanning electron microscopy, D, transmission electron microscopy (TEM), and, E, High-resolution TEM (HRTEM) images of the BiSb@C. F, Cycling performance of Bi@C, Sb@C and BiSb@C electrodes. G, Operando XRD results of BiSb@C anode during the first and second cycles and the proposed potassium storage mechanism. Reproduced with permission from Reference 86, Copyright 2020, American Chemical Society

matrix not only prevented the aggregation of SnSb particles but also acted as a 3D conductive network to facilitate electron and ions transfer. In addition, the defective carbon could provide extra active sites for potassium storage. Thus, the SnSb@NC composite anodes delivered an improved electrochemical performance in PIBs.

## 4 | ANTIMONY CHALCOGENIDES

Apart from the metallic Sb anodes, antimony chalcogenides such as antimony oxides, antimony sulfides, and antimony selenides have also attracted intense interests owing to several advantages. First, a large proportion of Sb element exists in the earth's crust in the form of antimony sulfides, and the metallic Sb is mostly obtained by the reduction of the antimony chalcogenides in industry. So, using antimony chalcogenides as anodes is more cost-effective compared to metallic Sb. Secondly, based on the conversion-alloying mechanism, the theoretical capacities of antimony chalcogenides are higher than that of metallic Sb.[89] Thirdly, it is easy to prepare antimony sulfides and selenides with different nanoarchitectures such as 1D nanorods and 2D nanosheets.[90] By contrast, metallic Sb has been mainly explored as 0D nanoparticles in the recent literatures. However, similar to the metallic Sb-based anodes, the conversion-alloying type electrode materials also suffer from inherent large volume variations during potassiation and depotassiation. Besides, the less-conductive discharge products from the conversion reaction stagnate the reaction kinetics, and some of the discharge products like potassium oxides are irreversible in the charging process.[91]

Among the antimony chalcogenides, antimony trisulfide ($Sb_2S_3$) stands out because of its high theoretical capacity (946 mAh $g^{-1}$) and better reversibility compared to antimony oxides.[92] The electrochemical mechanism of $Sb_2S_3$ in PIBs was also investigated by Guo's group via operando synchrotron X-ray diffraction and ex situ selected area electron diffraction patterns, and its potassiation process could be divided into the $K^+$ intercalation reaction, and then conversion and alloying reactions.[93] The total reaction equation can be summarized as follows:

$$Sb_2S_3 + 8K^+ + 8e^- \rightarrow 2K_3Sb + K_2S_3. \quad (1)$$

Based on the electrochemical reaction, the total volume change is estimated to be around ~300%. To overcome this problem and improve limited ion/charge transfer, they constructed a 2D $Sb_2S_3$/carbon (SBS/C) hybrid via a solution-triggered high-shear exfoliation process. The SBS/C with a few-layered structure was of great benefit for mitigating the volume expansion as well as accelerating the ion and electron transport during the repeated insertion and extraction of $K^+$ (Figure 7A,B). In addition, the carbon nanosheets protect the active material from loss by trapping the elemental S that is inevitably formed owing to the irreversible reaction between $Sb_2S_3$ and $K_2S_3$. Thus, the as-prepared $Sb_2S_3$/C anode delivered a specific capacity of 404 mAh $g^{-1}$ after 200 cycles at 500 mA $g^{-1}$ and retained 76% of the initial capacity when current densities were increased from 50 to 500 mA $g^{-1}$ (Figure 7C).

Antimony selenide ($Sb_2Se_3$) with a specific capacity of 670 mAh $g^{-1}$ has also been investigated as anodes for PIBs. Qian et al developed a hollow $Sb_2Se_3$@C microtube via a self-templated process for potassium storage.[95] The hollow $Sb_2Se_3$ core offers ample free space for accommodating the volume expansion, and the outer carbon layer not only provides extra mechanical protection to release the stress generated by the $Sb_2Se_3$ core but also prevents the aggregation of the $Sb_2Se_3$. Besides, 1D structures with carbon outer layer facilitates charge transfer and ion diffusion kinetics. As a result, the $Sb_2Se_3$@C electrode delivered a capacity of 313 mAh $g^{-1}$ at 100 mA $g^{-1}$ over 40 cycles, and a rate capability of 223 mAh $g^{-1}$ at 1 A $g^{-1}$. In situ Raman spectra and ex situ XRD results revealed that $K_2Se$ and Sb were first formed from the conversion during $K^+$ insertion, followed by an alloying process with the formation of $K_3Sb$. The depotassiation process was exactly opposite to the potassiation route. So the overall electrochemical reaction of $Sb_2Se_3$ was proposed to be as follows:

$$Sb_2Se_3 + 12K^+ + 12e^- \leftrightarrow 2K_3Sb + 3K_2Se. \quad (2)$$

Apart from the aforementioned antimony chalcogenides, Sb-based bimetallic oxides and sulfides inherit the merits of the alloy materials and enable a better electrochemical performance than the monometallic counterparts. Lu's group conducted some pioneering works in this direction. They prepared (Bi, Sb)$_2S_3$ nanotubes via a simple coprecipitation method, in which the ratio of Bi-Sb could be facilely regulated.[94] Interestingly, an in situ alloying strategy to form uniform (Bi, Sb) alloy nanoparticles was discovered, which can deliver exceptional performances in PIBs. The $K^+$ intercalation proceeds first, and then $Sb^{3+}$ and $Bi^{3+}$ are reduced in situ to form BiSb alloy during discharging. It is an atomic-level alloying process, generating a more homogenous distribution of Bi and Sb compared with that synthesized by the conventional routes. This conversion reaction from (Bi, Sb)$_2S_3$ to (Bi, Sb) alloy is irreversible, and the subsequent potassiation process is the same as in the BiSb alloy anodes mentioned in the previous section. As shown in Figure 7D, the phase transformation during the insertion

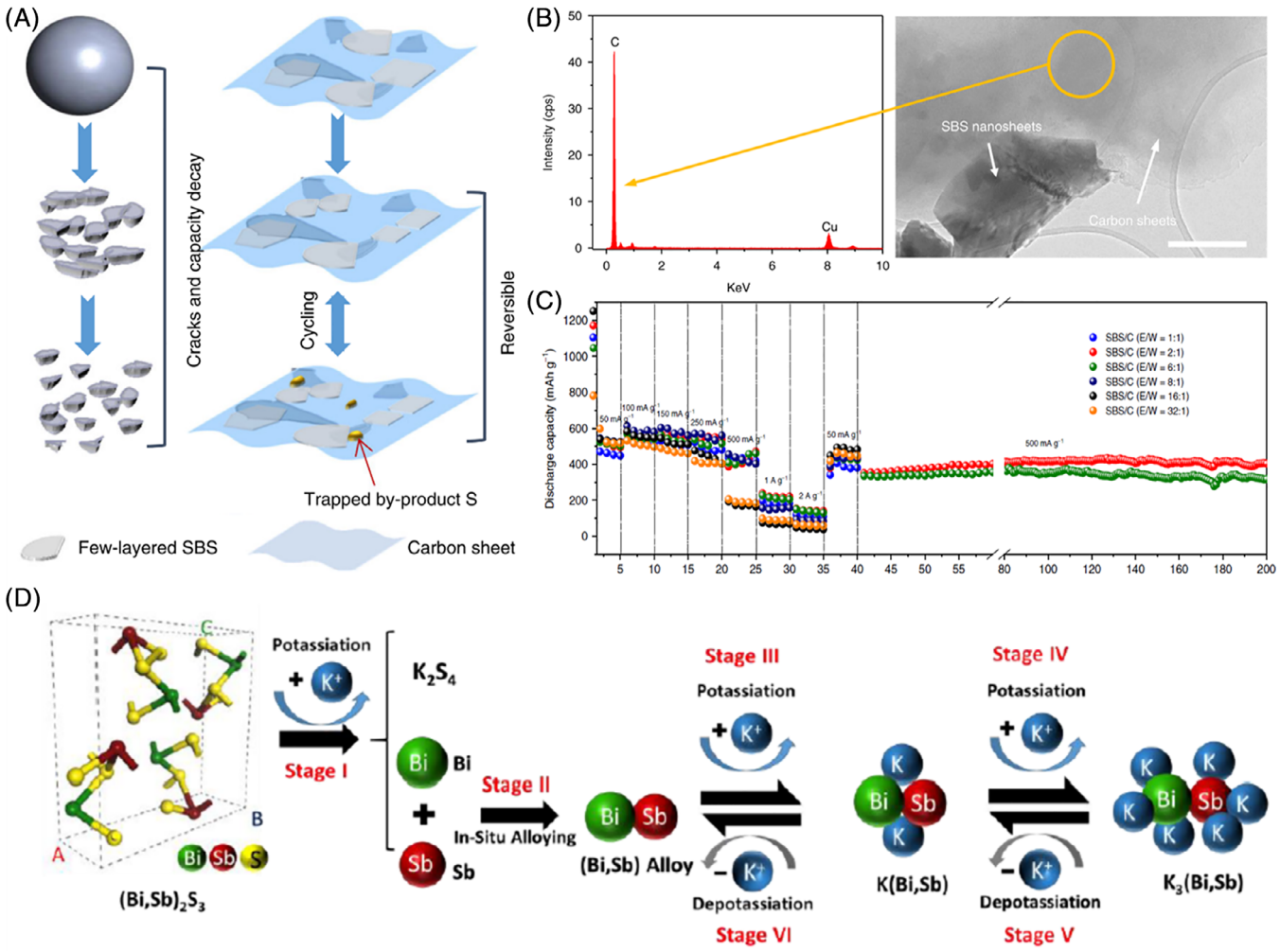


**FIGURE 7** A, Schematic illustration of the structural change of bulk $Sb_2S_3$ and few-layered $Sb_2S_3$/carbon (SBS/C) electrodes. (B) TEM image of the SBS/C composite and corresponding energy disperse spectroscopy spectrum of the indicated area. Scale bars: 200 nm. C, Rate capabilities of SBS/C electrodes exfoliated with different solvents obtained at the various charge and discharge current densities and their cycling performance after rate testing at 500 mA $g^{-1}$. Reproduced with permission from Reference 93, Copyright 2018, Nature Publication Group. D, Schematic illustration of the potassiation/depotassiation process in $(Bi,Sb)_2S_3$. Reproduced with permission from Reference 94, Copyright 2019, American Chemical Society

and extraction of $K^+$ was concluded to be: $(Bi,Sb)_2S_3 \rightarrow (Bi,Sb) \leftrightarrow K(Bi,Sb) \leftrightarrow K_3(Bi,Sb)$. These electrodes delivered a capacity of 353 mAh $g^{-1}$ at 0.5 A $g^{-1}$ after 1000 cycles, and a rate capacity of 300 mAh $g^{-1}$ at 1 A $g^{-1}$. More recently, the same group reported 2D $Sb_2MoO_6$/rGO nanosheets for PIBs, which exhibited a much better rate and cycling performance than those of the Sb- and Mo-based oxides/rGO.[96] However, the specific capacity is inferior in comparison with the $(Bi,Sb)_2S_3$ due to the incorporation of inactive Mo.

As an overview in Table 1 we have summarized the initial coulombic efficiencies (ICEs), rate capabilities and cycling performances of PIBs with the reported metallic Sb and Sb-based composite anodes. The corresponding compositions, structural properties, synthetic methods, and electrolyte formulation are presented as well. In general, a hierarchical structure that can combine the fast reaction kinetics and good electrode structural stability are of top priority for realizing superior potassium storage performance. This can be achieved by a multistep electrode material engineering approach. For example, we fabricated a high performance antimony selenide ($Sb_2Se_3$) composite anode for PIBs through a combined strategy of conductive encapsulation and 2D confinement.[97] The $Sb_2Se_3$ nanorods are uniformly coated with a conductive N-doped carbon layer and then confined between graphene nanosheets. The synergistic effects between conductive coating and confinement effectively facilitate the electron transport and ion diffusion, buffer the large volumetric variation, and maintain the structural stability for superior cyclability.

**TABLE 1** Comparison of the compositions, structural properties, synthetic methods, electrolytes, and electrochemical performances of the Sb and Sb-based composite anodes in potassium-ion batteries

| Anode | Synthetic methods | Electrolyte | ICE (%) | Rate performance | Cycling performance | Retention (%) | References |
|---|---|---|---|---|---|---|---|
| Sb/C | Ball-milling | 1 M $KPF_6$ in PC/EC | 74 | 440 $mAhg^{-1}$ at 0.175 A $g^{-1}$ | 590 mAh $g^{-1}$ after 10 cycles | 90 | 38 |
| Sb/graphite | Ball-milling and ultrasonication | 1 M KFSI in EMC | 91.6 | 238 mAh $g^{-1}$ at 2 A $g^{-1}$ | 449 mAh $g^{-1}$ at 0.2 A $g^{-1}$ after 100 cycles | 97 | 61 |
| Sb/CNFs | Electrospinning | 0.8 M $KPF_6$ in EC/DEC | 50 | 161 mAh $g^{-1}$ at 1 A $g^{-1}$ | 266 mAh $g^{-1}$ at 0.05 A $g^{-1}$ after 50 cycles | 93 | 62 |
| Sb@N-doped CNF | Electrospinning | 1.0 M KFSI in EC/DEC | 46 | 212 mAh $g^{-1}$ at 5 A $g^{-1}$ | 360 mAh $g^{-1}$ at 0.05 A $g^{-1}$ after 200 cycles | 60 | 63 |
| Sb@hollow CNFs | Template-assisted electrospinning | 3 M KFSI in DME | 48.3 | 145 mAh $g^{-1}$ at 5 A $g^{-1}$ | 225 mAh $g^{-1}$ at 1 A $g^{-1}$ after 2000 cycles | 93 | 64 |
| Sb nanorod@ hollow CNT | Hydrothermal | 1.0 M KFSI in EC/DMC | 70 | 211 mAh $g^{-1}$ at 5 A $g^{-1}$ | 300 mAh $g^{-1}$ at 2 A $g^{-1}$ after 120 cycles | 74 | 50 |
| Sb NPs | Thermal reduction | 0.8 M $KPF_6$ in PC/EC | 62.3 | 190 mAh $g^{-1}$ at 1 A $g^{-1}$ | 75 mAh $g^{-1}$ at 0.05 A $g^{-1}$ after 40 cycles | 20 | 53 |
| SbNPs/ graphene | Sonication | 0.8 M $KPF_6$ in PC/EC | 44 | 172 mAh $g^{-1}$ at 2 A $g^{-1}$ | 210 mAh $g^{-1}$ at 0.5 A h $g^{-1}$ after 200 cycles | 80 | 53 |
| Sb/CNS | Solvothermal | 1.0 M $KPF_6$ in EC/DMC | 48 | 101 mAh $g^{-1}$ at 2 A $g^{-1}$ | 247 mAh $g^{-1}$ at 0.2 A $g^{-1}$ after 600 cycles | 90 | 73 |
| MXene@Sb | Electrodeposition | 5.0 M KFSI in DME | 62.5 | 270 mAh $g^{-1}$ at 0.5 A $g^{-1}$ | 215 mAh $g^{-1}$ at 0.5 A $g^{-1}$ after 500 cycles | 79 | 77 |
| Micro-sized porous Sb | Vacuum distillation | 0.8 M $KPF_6$ in EC/DEC | 71 | 265 mAh $g^{-1}$ at 0.5 A $g^{-1}$ | 318 mAh $g^{-1}$ at 0.1 A $g^{-1}$ after 50 cycles | 62 | 56 |
| SbNPs@3D Carbon | Freeze-drying | 0.8 M $KPF_6$ in EC/DEC | 70 | 288 mAh $g^{-1}$ at 1 A $g^{-1}$ | 225 mAh $g^{-1}$ at 1 A $g^{-1}$ after 50 cycles | 80 | 48 |
| Sb@C-3D Porous | KCl template | 5.0 M KFSI in DME | 76.2 | 286 mAh $g^{-1}$ at 1 A $g^{-1}$ | 342 mAh $g^{-1}$ at 0.5 A $g^{-1}$ after 260 cycles | 97 | 66 |
| Sb@Carbon Sphere | Electrospray | 4.0 M KFSI in EC/DEC | 63 | 530 mAh $g^{-1}$ at 0.2 A $g^{-1}$ | 504 mAh $g^{-1}$ at 0.2 A $g^{-1}$ after 220 cycles | 81 | 52 |
| 2D $Sb_2S_3$/C | High-shear exfoliation | 1.0 M $KSiF_6$ in PC/EC | 50 | 140 mAh $g^{-1}$ at 2 A $g^{-1}$ | 174 mAh $g^{-1}$ at 1 A $g^{-1}$ after 1000 cycles | 79 | 93 |
| $Sb_2Se_3$@C microtube | A self-templated route | 0.8 M $KPF_6$ in PC/EC | 48.8 | 233 mAh $g^{-1}$ at 1 A $g^{-1}$ | 191 mAh $g^{-1}$ at 0.5 A $g^{-1}$ after 400 cycles | 75 | 94 |
| $Bi_{1.11}Sb_{0.89}S_3$ | Coprecipitation | 3 M KFSI in DME | 59.8 | 300 mAh $g^{-1}$ at 1 A $g^{-1}$ | 353 mAh $g^{-1}$ at 0.5 A $g^{-1}$ after 1000 cycles | 78 | 95 |
| SnSb | Ball-milling | 0.8 M KFSI in EC/DEC | 77 | 375 mAh $g^{-1}$ at 0.022 A $g^{-1}$ | 282 mAh $g^{-1}$ at 0.02 A $g^{-1}$ after 40 cycles | 76 | 41 |
| SnSb@ 3D porous C | NaCl template pyrolysis | 0.5 M $KPF_6$ in DME | 90.1 | 156 mAh $g^{-1}$ at 1 A $g^{-1}$ | 185.8 mAh $g^{-1}$ at 0.5 A $g^{-1}$ after 200 cycles | 80 | 88 |
| BiSb@C | Pyrolysis | 5 M KFSI in DME | 70.2 | 152 mAh $g^{-1}$ at 2 A $g^{-1}$ | 320 mAh $g^{-1}$ at 0.5 A $g^{-1}$ after 600 cycles | 97 | 86 |
| $MoS_2$@Sb@C | Hydrothermal and sulfidation | 1 M KFSI in DEGDME | 59.3 | 235 mAh $g^{-1}$ at 2 A $g^{-1}$ | 296 mAh $g^{-1}$ at 0.5 A $g^{-1}$ after 200 cycles | 94 | 82 |
| 3D FeSb@N-doped C | Freeze-drying and Pyrolysis | 0.8 M $KPF_6$ in EC/DEC | 52 | 120 mAh $g^{-1}$ at 2 A $g^{-1}$ | 135 mAh $g^{-1}$ at 0.5 A $g^{-1}$ after 1000 cycles | 85 | 85 |
| 2D $Sb_2MoO_6$/rGO | Hydrothermal | 3 M KFSI in DME | 55.7 | 161 mAh $g^{-1}$ at 1 A $g^{-1}$ | 247 mAh $g^{-1}$ at 0.5 A $g^{-1}$ after 100 cycles | 99 | 96 |

Abbreviations: CNT, carbon nanotube; CNF, carbon nanofiber; DEC, diethylene carbonate; DME, dimethoxyethane; DEGDME, diethlyene glycol dimethyl ether; DMC, dimethyl carbonate, EC, ethylene carbonate; EMC, ethyl methyl carbonate; ICE, initial coulombic efficiency; KFSI, potassium bis(fluorosulfonyl)imide-dimethoxyethane; $KPF_6$, potassium hexafluorophosphate; PC, propylene carbonate; PIB, potassium-ion battery; rGO, reduced graphene oxide.

## 5 | OPTIMIZATION OF THE ELECTROLYTES AND ELECTRODE FORMULATION

The electrolyte plays a more important role in PIBs than in LIBs and SIBs because of the violent side reactions between electrolytes and highly reactive metallic potassium. An optimized electrolyte, including types and specific concentrations of potassium salts, solvents and additives, has a great influence on the formation of SEI layer and the prevention of side reactions, which are crucial to Coulombic efficiency and cycle life of the PIBs.[98-100] For example, Guo et al demonstrated that KFSI in carbonate electrolyte could induce a more mechanically robust, uniform and conductive SEI layer than potassium hexafluorophosphate ($KPF_6$) in alloy-based anodes (Figure 8A-C), which suppressed the decomposition of the electrolytes, reduced side reactions and maintained electrode integrity.[101] The worst aspect of using $KPF_6$ might be ascribed to the formation of strong Lewis acid by decomposition or hydrolysis of the salt ($KPF_6 \rightarrow KF + PF_5$, $KPF_6 + H_2O \rightarrow KF + HF + POF_3$), which induces the polymerization of ethylene carbonate (EC) and side reactions with the discharge product.[102] As shown in Figure 8D, the Sb/C electrodes delivered a significantly improved cycling capacity (470 mAh $g^{-1}$ after 50 cycles) in KFSI carbonate electrolyte compared with the $KPF_6$ electrolyte (80 mAh $g^{-1}$ after 15 cycles).

Madec et al systematically investigated the electrolyte reactivity in K metal/Sb half cells and its influences on the formation of the electrode/electrolyte interphase.[103] It has been proved that the Coulombic efficiency increased by the addition of fluoroethylene carbonate (FEC) and vinylene carbonate (VC) to propylene carbonate (PC), the replacement of PC by EC/diethylene carbonate (DEC), and the replacement of $KPF_6$ by KFSI. Furthermore, optical observations of deassembled postcycled electrodes coupled with gas chromatography-mass spectrometry and X-ray photoelectron spectroscopy (XPS) results reveal that the species from the reaction between K metal and electrolyte can migrate to the anode side and affect the Sb/electrolyte interphase via a cross-talk mechanism. This work indicated the necessity of employing full cells to evaluate the electrochemical performance for excluding the influences of K metal when we search for new electrolytes.

To achieve better electrochemical performances of Sb-based anodes, it is necessary to combine the investigation of nanoarchitectural design and electrolyte regulation.[104] Wang et al prepared an Sb@CSN composite electrode with Sb nanoparticles uniformly encapsulated in carbon spheres via a scalable electrospray technique.[50] Furthermore, they also regulated the components of ester-based electrolytes to facilitate the formation of a stable KF-rich SEI layer (an inorganic-dominated SEI layer) on the anodes. The well-defined Sb@CSN electrode in the optimized 4 M KTFSI electrolyte delivered a discharge capacity of 626 mAh $g^{-1}$ at the second cycle with a low capacity decay from the 10th to 100th cycle, stabilizing at 504 mAh $g^{-1}$ at 200 mA $g^{-1}$ after 220 cycles (Figure 8E). The improvement of the electrochemical performance ascribed to not only the delicate nanostructure design but also the optimized electrolyte (4 M KTFSI/EC + DEC).

The composition of SEI films was characterized by in-depth XPS as shown in Figure 8F. The merits of concentrated KTFSI electrolyte are summarized as follows: (a) the concentrated KTFSI electrolyte with abundant F element can reach and participate in SEI formation more easily compared with the dilute counterpart. Accompanied with concentrated $K^+$, a KF-rich SEI layer was generated; (b) A robust KF-rich SEI layer could guard against further reaction between the active materials and the electrolyte, at same time accommodating the volume change of active materials, thereby an excellent K-storage performance can be reached; and (c) concentrated KTFSI could prevent the KF from dissolving the electrolyte as well, further stabilizing the SEI layer for good cycling performance (Figure 8G).

Apart from the ester-based electrolytes, ether-based electrolytes were found to be more stable in some cases. For example, a thinner SEI film was formed on SnSb@NC electrode in DME-based electrolyte rather than EC/DEC electrolyte.[88] By contrast, the decomposition of the ester electrolyte was more serious, leading to the formation of a thicker SEI film and larger charge transfer resistance. Thus, the SnSb@NC electrode based on $KPF_6$ in DME electrolyte delivered an improved rate capability and cycling performance compared to the EC/DEC electrolyte.

In addition, binders and carbon additives are two other factors which need to be considered for the improvement of the electrochemical performance of Sb electrodes in PIBs. Glushenkov et al also demonstrated that biodegradable polymer gum arabic (composed of a polysaccharide and glycoproteins) is much better than the conventional carboxymethyl cellulose and could enhance the mechanical properties and tolerate volume expansion stress of the electrodes during cycling.[60] Monconduit et al investigated the effects of carbon additives on electrode formulation of bulk Sb in PIBs.[105] They found that double-walled carbon nanotubes (DWCNT) were a better conductive additive compared with conventional carbon black, graphite, vapor ground carbon fibers, and super P. This is because DWCNT also acted as a mechanical reinforcement for the whole electrode that could withstand the volume change of Sb.

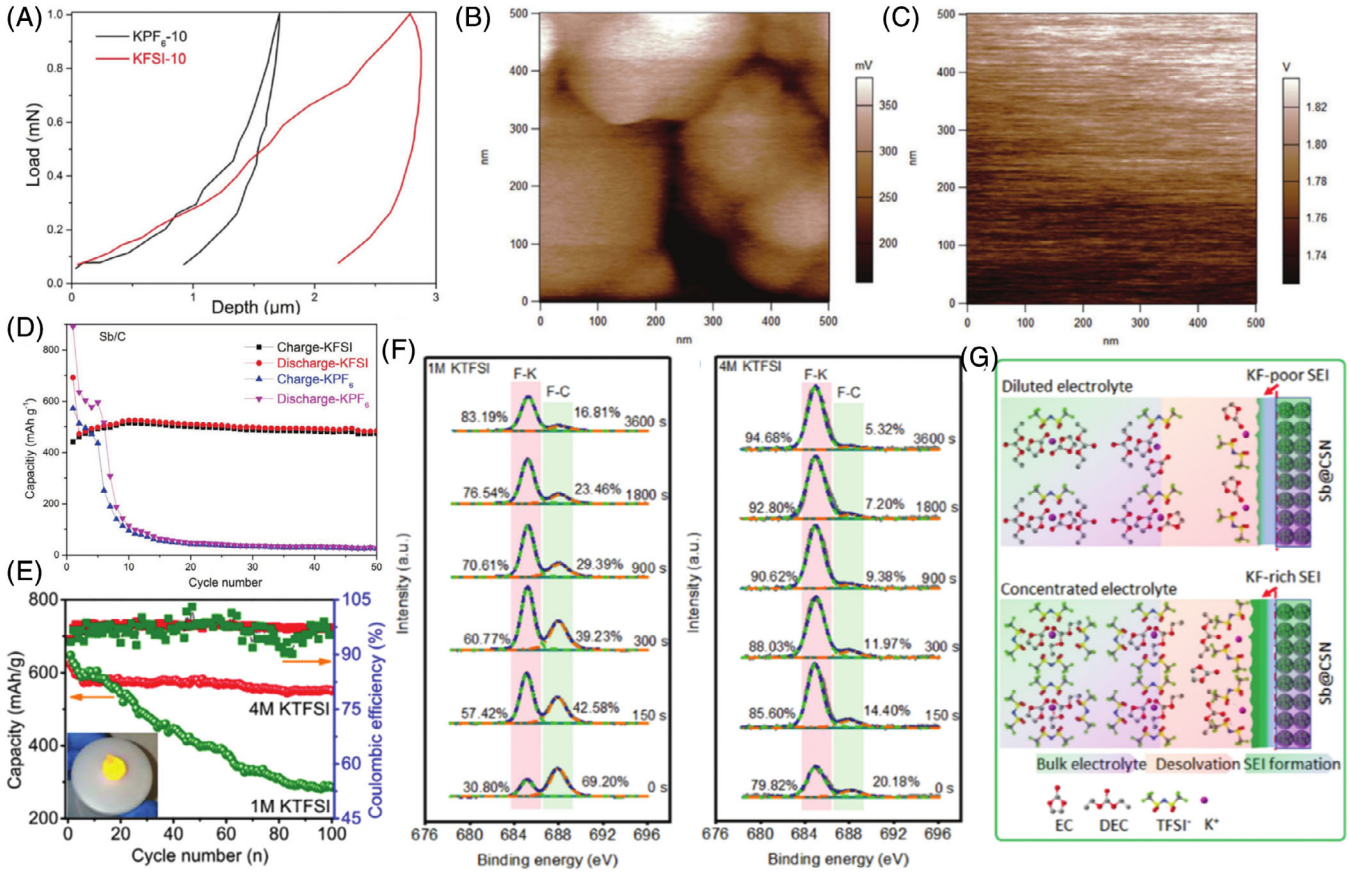


**FIGURE 8** A, Nanoindentation force of the alloy anode at a given indentation depth after cycling in potassium hexafluorophosphate ($KPF_6$) and potassium bis(fluorosulfonyl)imide (KFSI) electrolyte, respectively. Surface potential maps of the electrode for, B, $KPF_6$ electrolyte and, C, KFSI electrolyte, respectively. D, The cycling performance of Sb/C electrodes in $KPF_6$ and KFSI electrolytes at 50 mA $g^{-1}$. Reproduced with permission from Reference 101, Copyright 2019, Wiley-VCH. E, Cycling performance of the Sb@CSN electrode at 100 mA $g^{-1}$ in different electrolytes. F, In-depth X-ray photoelectron spectroscopy (XPS) spectra in the F1s region for the Sb@CSN electrode in 1 M and 4 M potassium trifluoromethane-sulfonimide (KTFSI) electrolyte. G, Illustration of the influence of dilute and concentrated electrolytes on the formation of the solid electrolyte interface (SEI) layer. Reproduced with permission from Reference 50, Copyright 2019, Royal Society of Chemistry

## 6 | SUMMARY AND OUTLOOK

In this review, we systematically reviewed and summarized recent progress on Sb and Sb-based alloys as anodes for PIBs. Antimony, with its high theoretical capacity and appropriate potassiation potential, is regarded as a promising alloying-type anode material for PIBs. However, the large volume change of Sb electrode during potassiation/depotassiation processes leads to inferior cycling performance and impedes their practical application. To address these issues, enormous efforts have been devoted to nanoengineering Sb structure, combining Sb with complementary conductive matrixes, alloying and fabrication of hierarchically porous nanocomposites. Those strategies have demonstrated capability for effectively buffering the volume changes of Sb, facilitating the electronic and ionic conductivity, and boosting the electrochemical kinetics during charge and discharge, thereby resulting in enhanced rate capability and cycling performance. Besides the metallic Sb, antimony chalcogenides have also been considered as promising anode materials for PIBs owing to their high theoretical capacities and low cost. Furthermore, the morphology of those metal sulfides/selenides can be easier controlled by either a bottom-up or top-down approach compared to metallic Sb, which is advantageous for electrode fabrication.

Apart from the optimization of Sb-based materials, electrolyte composition is another significant factor that determines the formation of SEI layer and has a great influence on the cycling performance of potassium storage as well. Particularly, an appropriate electrolyte can reduce side reactions between super-reactive K and the electrolyte and improve the Coulombic efficiencies of the PIBs. In addition, the battery performance can also be enhanced by modulating other elements in the electrode formulation, such as binders and carbon additives.

Although great advances of Sb-based anodes has been reported for potassium storage in the past few years, further investigations are still needed to accelerate the practical application of PIBs. These include:

1 Despite the fact that the potassium storage mechanisms have been widely reported in many publications, few studies investigated battery failure mechanism in detail. In-depth studies are essential to comprehensively understand the failure mechanism of Sb-based electrodes, which can guide effective future electrode design. It is worth noting that the degradation of metallic potassium may be even more severe than that of Sb-based anodes in half cells.[81] Thus, more attention should be paid to the influence of metallic potassium as counter electrodes on the capacity decay. To circumvent this issue, full cells should be assembled for evaluating electrochemical performance.[103]
2 The study of alloying methods to improve performance should not be limited to those elements which can form alloys with Sb. Previous work showed that simple mixed Sb with black phosphorous could largely enhance the cycling performance even though the two components do not alloy with each other.[60] Besides, in situ alloying during the electrochemical reaction is another route which should be considered to buffer the volume change of Sb during charge and discharge.[94] Particularly, these types of materials that are active with potassium might have synergistic effects for stabilizing the electrode structure as well as increasing cell capacity.
3 Using nanoarchitectures to alleviate the huge volume expansion of the Sb-based anodes inevitably lower the tap density of the electrode materials and volume density of the final devices. The mechanical stress derived from the volume change would become more serious at high load, leading to faster degradation of the electrode. Thus, the future research should pay attention to the electrochemical performance in high load as well. We can conclude that the composite anode materials with metallic antimony or antimony chalcogenides as complementary building blocks to graphite and other conductive matrixes make a good balance of capacity and cycling stability, which are preferable for practical application.
4 The modulation of electrolyte has a key impact on the electrochemical performance of PIBs. An optimized electrolyte could not only have a high ionic conductivity but also contribute to formation of a robust and conductive SEI on both cathode and anode sides. More efforts should be devoted to developing low cost, stable, and safe electrolytes for high performance alloy-based anodes and investigating the underpinning mechanisms.

We hope these perspectives can bring some inspirations to researchers in the field and promote the development of anode materials for PIBs. The nanoengineering methodologies that we have summarized for improving the performance of Sb-based anodes can also be applied to modify many other conversion and alloying type electrode materials for rechargeable batteries.

## ACKNOWLEDGMENTS

This work was financially supported by the Australian Research Council (ARC) through the Discovery Project program (DP180102297) and ARC Research Hub for Integrated Energy Storage Solutions (IH180100020). H. G. appreciates the support from the China Postdoctoral Science Foundation Funded Project (2019M661464).

## ORCID

*Xin Guo* https://orcid.org/0000-0001-7771-0463
*Guoxiu Wang* https://orcid.org/0000-0003-4295-8578

## REFERENCES

1. Dunn B, Kamath H, Tarascon J-M. Electrical energy storage for the grid: a battery of choices. *Science*. 2011;334:928-935.
2. Yang Z, Zhang J, Kintner-Meyer MCW, et al. Electrochemical energy storage for green grid. *Chem Rev*. 2011;111:3577-3613.
3. Guo X, Sun B, Su D, et al. Recent developments of aprotic lithium-oxygen batteries: functional materials determine the electrochemical performance. *Sci Bull*. 2017;62:442-452.
4. Su D, McDonagh A, Qiao SZ, Wang G. High-capacity aqueous potassium-ion batteries for large-scale energy storage. *Adv Mater*. 2017;29:1-8.
5. Zhang W, Hu C, Guo Z, Dai L. High-performance K-$CO_2$ batteries based on metal-free carbon electrocatalysts. *Angew Chem Int Ed*. 2020;59:3470-3474.
6. Okoshi M, Yamada Y, Komaba S, Yamada A, Nakai H. Theoretical analysis of interactions between potassium ions and organic electrolyte solvents: a comparison with lithium, sodium, and magnesium ions. *J Electrochem Soc*. 2017;164: A54-A60.
7. Zhang W, Liu Y, Guo Z. Approaching high-performance potassium-ion batteries via advanced design strategies and engineering. *Sci Adv*. 2019;5: eaav7412.
8. Eftekhari A, Jian ZL, Ji XL. Potassium secondary batteries. *ACS Appl Mater Interfaces*. 2017;9:4404-4419.
9. Zhao S, Yan K, Munroe P, et al. Construction of hierarchical $K_{1.39}Mn_3O_6$ spheres via $AlF_3$ coating for high-performance potassium-ion batteries. *Adv Energy Mater*. 2019;9:1803757.
10. Y Zhao Y, Zhu J, Ong SJH, et al. High-rate and ultralong cycle-life potassium ion batteries enabled by in situ engineering of yolk–shell $FeS_2$@C structure on graphene matrix. *Adv Energy Mater* 2018;8:1802565.
11. Zhou J, Ye L, Zhang S, Zhou T, Guo Z. Metal chalcogenides for potassium storage. *InfoMat*. 2020;2:437–465. https://doi.org/10.1002/inf2.12101.
12. Tang X, Zhou D, Li P, et al. MXene-based dendrite-free potassium metal batteries. *Adv Mater*. 2020;32:1906739.

13. Pramudita JC, Sehrawat D, Goonetilleke D, Sharma N. An initial review of the status of electrode materials for potassium-ion batteries. *Adv Energy Mater*. 2017;7:1602911.
14. Zhao J, Zou XX, Zhu YJ, Xu Y, Wang C. Electrochemical intercalation of potassium into graphite. *Adv Funct Mater*. 2016;26:8103-8110.
15. Fan L, Ma R, Zhang Q, Jia X, Lu B. Graphite anode for a potassium-ion battery with unprecedented performance. *Angew Chem Int Ed*. 2019;58:10500-10505.
16. Luo W, Wan JY, Ozdemir B, et al. Potassium ion batteries with graphitic materials. *Nano Lett*. 2015;15:7671-7677.
17. Jian Z, Luo W, Ji X. Carbon electrodes for K-ion batteries. *J Am Chem Soc*. 2015;137:11566-11569.
18. Jian ZL, Hwang S, Li ZF, et al. Hard-soft composite carbon as a long-cycling and high-rate anode for potassium-ion batteries. *Adv Funct Mater*. 2017;27:1700324.
19. Xu Y, Zhang C, Zhou M, et al. Highly nitrogen doped carbon nanofibers with superior rate capability and cyclability for potassium ion batteries. *Nat Commun*. 2018;9:1720.
20. Hao R, Lan H, Kuang C, Wang H, Guo L. Superior potassium storage in chitin-derived natural nitrogen-doped carbon nanofibers. *Carbon*. 2018;128:224-230.
21. Zhao S, Dong L, Sun B, et al. $K_2Ti_2O_5$@C microspheres with enhanced $K^+$ intercalation pseudocapacitance ensuring fast potassium storage and long-term cycling stability. *Small*. 2020;16:1906131.
22. Guo X, Xie X, Choi S, et al. $Sb_2O_3$/MXene($Ti_3C_2T_x$) hybrid anode materials with enhanced performance for sodium-ion batteries. *J Mater Chem A*. 2017;5:12445-12452.
23. Ren X, Zhao Q, McCulloch WD, Wu Y. $MoS_2$ as a long-life host material for potassium ion intercalation. *Nano Res*. 2017;10:1313-1321.
24. Gao H, Zhou T, Zheng Y, et al. CoS quantum dot nanoclusters for high-energy potassium-ion batteries. *Adv Funct Mater*. 2017;27:1702634.
25. Lakshmi V, Chen Y, Mikhaylov AA, et al. Nanocrystalline $SnS_2$ coated onto reduced graphene oxide: demonstrating the feasibility of a non-graphitic anode with sulfide chemistry for potassium-ion batteries. *Chem Commun*. 2017;53:8272-8275.
26. Lian P, Dong Y, Wu Z-S, et al. Alkalized $Ti_3C_2$ MXene nanoribbons with expanded interlayer spacing for high-capacity sodium and potassium ion batteries. *Nano Energy*. 2017;40:1-8.
27. Zhang W, Pang WK, Sencadas V, Guo Z. Understanding high-energy-density $Sn_4P_3$ anodes for potassium-ion batteries. *Joule*. 2018;2:1534-1547.
28. Wang Q, Zhao X, Ni C, et al. Reaction and capacity-fading mechanisms of tin nanoparticles in potassium-ion batteries. *J Phys Chem C*. 2017;121:12652-12657.
29. Zhang R, Bao J, Wang Y, Sun C-F. Concentrated electrolytes stabilize bismuth-potassium batteries. *Chem Sci*. 2018;9:6193-6198.
30. Sultana I, Rahman MM, Chen Y, Glushenkov A. Potassium-ion battery anode materials operating through the alloying-dealloying reaction mechanism. *Adv Funct Mater*. 2017;28:1703857.
31. Zhang W, Mao J, Li S, Chen Z, Guo Z. Phosphorus-based alloy materials for advanced potassium-ion battery anode. *J Am Chem Soc*. 2017;139:3316-3319.
32. Song K, Liu C, Mi L, et al. Recent progress on the alloy-based anode for sodium-ion batteries and potassium-ion batteries. *Small*. 2019;15:1903194.
33. Yu S, Kim SO, Kim HS, Choi W. Computational screening of anode materials for potassium-ion batteries. *Int J Energy Res*. 2019;43:7646-7654.
34. Ruiz O, Cochrane M, Li M, et al. Enhanced cycling stability of macroporous bulk antimony-based sodium-ion battery anodes enabled through active/inactive composites. *Adv Energy Mater*. 2018;8:1801781.
35. He J, Wei YQ, Zhai TY, Li HQ. Antimony-based materials as promising anodes for rechargeable lithium-ion and sodium-ion batteries. *Mater Chem Front*. 2018;2:437-455.
36. Liu H, Liu X, Li W, et al. Porous carbon composites for next generation rechargeable lithium batteries. *Adv Energy Mater*. 2017;7:1700283.
37. Gao H, Yang F, Zheng Y, et al. Three-dimensional porous cobalt phosphide nanocubes encapsulated in a graphene aerogel as an advanced anode with high coulombic efficiency for high-energy lithium-ion batteries. *ACS Appl Mater Interfaces*. 2019;11:5373-5379.
38. McCulloch WD, Ren X, Yu M, et al. Potassium-ion oxygen battery based on a high capacity antimony anode. *ACS Appl Mater Interfaces*. 2015;7:26158-26166.
39. Guo X, Zhang J, Song J, Wu W, Liu H, Wang G. MXene encapsulated titanium oxide nanospheres for ultra-stable and fast sodium storage. *Energy Storage Mater*. 2018;14:306-313.
40. Wang H, Wu X, Qi XJ, Zhao W, Ju Z. Sb nanoparticles encapsulated in 3D porous carbon as anode material for lithium-ion and potassium-ion batteries. *Mater Res Bull*. 2018;103:32-37.
41. Gabaudan V, Berthelot R, Sougrati MT, Lippens PE, Monconduit L, Stievano L. SnSb vs. Sn: improving the performance of Sn-based anodes for K-ion batteries by synergetic alloying with Sb. *J Mater Chem A*. 2019;7:15262-15270.
42. Liu ZM, Song T, Paik U. Sb-based electrode materials for rechargeable batteries. *J Mater Chem A*. 2018;6:8159-8193.
43. Xiang J, Yang L, Yuan L, et al. Alkali-metal anodes: from lab to market. *Joule*. 2019;3:2334-2363.
44. Liu J, Yuan H, Tao X, et al. Recent progress on biomass-derived ecomaterials toward advanced rechargeable lithium batteries. *EcoMat*. 2020;2:12019.
45. Tan H, Chen D, Rui X, Yu Y. Peering into alloy anodes for sodium-ion batteries: current trends, challenges, and opportunities. *Adv Funct Mater*. 2019;29:1808745.
46. Lao M, Zhang Y, Luo W, Yan Q, Sun W, Dou SX. Alloy-based anode materials toward advanced sodium-ion batteries. *Adv Mater*. 2017;29:1700622.
47. Wang T, Su D, Shanmukaraj D, Rojo T, Armand M, Wang G. Electrode materials for sodium-ion batteries: considerations on crystal structures and sodium storage mechanisms. *Electrochem Energy Rev*. 2018;1:200-237.
48. Han C, Han K, Wang X, et al. Three-dimensional carbon network confined antimony nanoparticle anodes for high-capacity K-ion batteries. *Nanoscale*. 2018;10:6820-6826.
49. Luo W, Li F, Zhang WR, et al. Encapsulating segment-like antimony nanorod in hollow carbon tube as long-lifespan, high-rate anodes for rechargeable K-ion batteries. *Nano Res*. 2019;12:1025-1031.
50. Zheng J, Yang Y, Fan X, et al. Extremely stable antimony-carbon composite anodes for potassium-ion batteries. *Energ Environ Sci*. 2019;12:615-623.

51. Darwiche A, Marino C, Sougrati MT, Fraisse B, Stievano L, Monconduit L. Better cycling performances of bulk Sb in Na-ion batteries compared to Li-ion systems: an unexpected electrochemical mechanism. *J Am Chem Soc*. 2012;134:20805-20811.
52. Sangster J, Pelton A. The K-Sb (potassium-antimony) system. *J Phase Equilibria*. 1993;14:510-514.
53. Yi Z, Lin N, Zhang WQ, Wang W, Zhu Y, Qian Y. Preparation of Sb nanoparticles in molten salt and their potassium storage performance and mechanism. *Nanoscale*. 2018;10:13236-13241.
54. An Y, Tian Y, Ci L, Xiong S, Feng J, Qian Y. Micron-sized nanoporous antimony with tunable porosity for high-performance potassium-ion batteries. *ACS Nano*. 2018;12:12932-12940.
55. Liu J, Yang Z, Wang J, Gu L, Maier J, Yu Y. Three-dimensionally interconnected nickel–antimony intermetallic hollow nanospheres as anode material for high-rate sodium-ion batteries. *Nano Energy*. 2015;16:389-398.
56. Guo X, Sun B, Zhang J, Liu H, Wang G. Ruthenium decorated hierarchically ordered macro–mesoporous carbon for lithium oxygen batteries. *J Mater Chem A*. 2016;4:9774-9780.
57. Yang JL, Ju ZC, Jiang Y, et al. Enhanced capacity and rate capability of nitrogen/oxygen dual-doped hard carbon in capacitive potassium-ion storage. *Adv Mater*. 2018;30:1700104.
58. Yang C, Li W, Yang Z, Gu L, Yu Y. Nanoconfined antimony in sulfur and nitrogen co-doped three-dimensionally (3D) interconnected macroporous carbon for high-performance sodium-ion batteries. *Nano Energy*. 2015;18:12-19.
59. Luo W, Li F, Gaumet J-J, et al. Bottom-up confined synthesis of nanorod-in-nanotube structured Sb@N-C for durable lithium and sodium storage. *Adv Energy Mater*. 2018;8:1703237.
60. Sultana I, Rahman MM, Liu J, et al. Antimony-carbon nanocomposites for potassium-ion batteries: insight into the failure mechanism in electrodes and possible avenues to improve cyclic stability. *J Power Sources*. 2019;413:476-484.
61. Liu Q, Fan L, Chen S, et al. Antimony-graphite composites for a high-performance potassium-ion battery. *Energ Technol*. 2019;7:1900634.
62. Zhang WM, Miao WF, Liu XY, Li L, Yu Z, Zhang QH. High-rate and ultralong-stable potassium-ion batteries based on antimony-nanoparticles encapsulated in nitrogen and phosphorus co-doped mesoporous carbon nanofibers as an anode material. *J Alloy Compd*. 2018;769:141-148.
63. Liu D, Yang L, Chen Z, et al. Ultra-stable Sb confined into N-doped carbon fibers anodes for high-performance potassium-ion batteries. *Sci Bull*. 2020;65:1003–1012. https://doi.org/10.1016/j.scib.2020.03.019.
64. Ge XF, Liu SH, Qiao M, et al. Enabling superior electrochemical properties for highly efficient potassium storage by impregnating ultrafine Sb nanocrystals within nanochannel-containing carbon nanofibers. *Angew Chem Int Ed*. 2019;58:14578-14583.
65. Wang L, Jia JJ, Wu Y, Niu KM. Antimony/reduced graphene oxide composites as advanced anodes for potassium ion batteries. *J Appl Electrochem*. 2018;48:1115-1120.
66. Han Y, Li T, Li Y, et al. Stabilizing antimony nanocrystals within ultrathin carbon nanosheets for high-performance K-ion storage. *Energy Storage Mater*. 2019;20:46-54.
67. He XD, Liu ZH, Liao JY, et al. A three-dimensional macroporous antimony@carbon composite as a high-performance anode material for potassium-ion batteries. *J Mater Chem A*. 2019;7:9629-9637.
68. Pomerantseva E, Bonaccorso F, Feng X, Cui Y, Gogotsi Y. Energy storage: the future enabled by nanomaterials. *Science*. 2019;366:eaan8285.
69. Wu Y, Huang HB, Feng Y, Wu ZS, Yu Y. The promise and challenge of phosphorus-based composites as anode materials for potassium-ion batteries. *Adv Mater*. 2019;31:1901414.
70. Li P, Guo X, Wang S, et al. Two-dimensional Sb@$TiO_{2-x}$ nanoplates as a high-performance anode material for sodium-ion batteries. *J Mater Chem A*. 2019;7:2553-2559.
71. Cui J, Yao S, Lu Z, et al. Revealing pseudocapacitive mechanisms of metal dichalcogenide $SnS_2$/graphene-CNT aerogels for high-energy Na hybrid capacitors. *Adv Energy Mater*. 2018;8:1702488.
72. Guo X, Zhang W, Zhang J, et al. Boosting sodium storage in two-dimensional phosphorene/$Ti_3C_2T_x$ MXene nanoarchitectures with stable fluorinated interphase. *ACS Nano*. 2020;14:3651-3659.
73. Song J, Guo X, Zhang J, et al. Rational design of free-standing 3D porous MXene/rGO hybrid aerogels as polysulfide reservoirs for high-energy lithium–sulfur batteries. *J Mater Chem A*. 2019;7:6507-6513.
74. Nan J, Guo X, Xiao J, et al. Nanoengineering of 2D MXene-based materials for energy storage applications. *Small*. 2020;26:1902085.
75. Tang X, Guo X, Wu W, Wang G. 2D metal carbides and nitrides (MXenes) as high-performance electrode materials for lithium-based batteries. *Adv Energy Mater*. 2018;8:1801897.
76. Bao W, Tang X, Guo X, et al. Porous cryo-dried MXene for efficient capacitive deionization. *Joule*. 2018;2:778-787.
77. Tian Y, An YL, Xiong SL, Feng J, Qian Y. A general method for constructing robust, flexible and freestanding MXene@metal anodes for high-performance potassium-ion batteries. *J Mater Chem A*. 2019;7:9716-9725.
78. Wang Z, Gao H, Zhang Q, et al. Recent advances in 3D graphene architectures and their composites for energy storage applications. *Small*. 2019;15:1803858.
79. Li N, Liao S, Sun Y, Song HW, Wang CX. Uniformly dispersed self-assembled growth of $Sb_2O_3$/Sb@graphene nanocomposites on a 3D carbon sheet network for high Na-storage capacity and excellent stability. *J Mater Chem A*. 2015;3:5820-5828.
80. Liu Q, Fan L, Ma RF, et al. Super long-life potassium-ion batteries based on an antimony@carbon composite anode. *Chem Commun*. 2018;54:11773-11776.
81. Ko YN, Choi SH, Kim H, Kim HJ. One-pot formation of Sb-carbon microspheres with graphene sheets: potassium-ion storage properties and discharge mechanisms. *ACS Appl Mater Interfaces*. 2019;11:27973-27981.
82. Cao L, Zhang B, Xia H, et al. Hierarchical chrysanthemum-like $MoS_2$/Sb heterostructure encapsulated into N-doped graphene framework for superior potassium-ion storage. *Chem Eng J*. 2020;387:124060.
83. Liu Y, Zhu Y, Cui Y. Challenges and opportunities towards fast-charging battery materials. *Nat Energy*. 2019;4:540-550.

84. Zhang YF, Li M, Huang FB, et al. 3D porous Sb-Co nanocomposites as advanced anodes for sodium-ion batteries and potassium-ion batteries. *Appl Surf Sci*. 2020;499:143907.
85. Wang ZY, Dong KZ, Wang D, et al. Constructing N-doped porous carbon confined FeSb alloy nanocomposite with Fe-N-C coordination as a universal anode for advanced Na/K-ion batteries. *Chem Eng J*. 2020;384:123327.
86. Xiong PX, Wu JX, Zhou MF, Xu YH. Bismuth-antimony alloy nanoparticle@porous carbon nanosheet composite anode for high-performance potassium-ion batteries. *ACS Nano*. 2020; 14:1018-1026.
87. He M, Walter M, Kravchyk KV, Erni R, Widmer R, Kovalenko MV. Monodisperse SnSb nanocrystals for Li-ion and Na-ion battery anodes: synergy and dissonance between Sn and Sb. *Nanoscale*. 2015;7:455-459.
88. Wang ZY, Dong KZ, Wang D, et al. A nanosized SnSb alloy confined in N-doped 3D porous carbon coupled with ether-based electrolytes toward high-performance potassium-ion batteries. *J Mater Chem A*. 2019;7:14309-14318.
89. Wang BY, Deng ZW, Xia YT, et al. Realizing reversible conversion-alloying of Sb(V) in polyantimonic acid for fast and durable lithium- and potassium-ion storage. *Adv Energy Mater*. 2020;10:1903119.
90. Ou X, Yang C, Xiong X, et al. A new rGO-overcoated $Sb_2Se_3$ nanorods anode for $Na^+$ battery: in situ X-ray diffraction study on a live sodiation/desodiation process. *Adv Funct Mater*. 2017;27:1606242.
91. Lu Y, Yu L, Lou XW. Nanostructured conversion-type anode materials for advanced lithium-ion batteries. *Chem*. 2018;4: 972-996.
92. Xiong X, Wang G, Lin Y, et al. Enhancing sodium ion battery performance by strongly binding nanostructured $Sb_2S_3$ on sulfur-doped graphene sheets. *ACS Nano*. 2016;10:10953-10959.
93. Liu Y, Tai Z, Zhang J, et al. Boosting potassium-ion batteries by few-layered composite anodes prepared via solution-triggered one-step shear exfoliation. *Nat Commun*. 2018;9:3645.
94. Wang J, Fan L, Liu ZM, et al. In situ alloying strategy for exceptional potassium ion batteries. *ACS Nano*. 2019;13:3703-3713.
95. Yi Z, Qian Y, Tian J, Shen KZ, Lin N, Qian YT. Self-templating growth of $Sb_2Se_3$@C microtube: a convention-alloying-type anode material for enhanced K-ion batteries. *J Mater Chem A*. 2019;7:12283-12291.
96. Wang J, Wang B, Liu ZM, et al. Nature of bimetallic oxide $Sb_2MoO_6$/rGO anode for high-performance potassium-ion batteries. *Adv Sci*. 2019;6:1900904.
97. Wang S, Xiong P, Guo X, et al. A stable conversion and alloying anode for potassium-ion batteries: a combined strategy of encapsulation and confinement. *Adv Funct Mater*. 2020;30:2001588. https://doi.org/10.1002/Adam.202001588.
98. Lei Y, Qin L, Liu R, et al. Exploring stability of nonaqueous electrolytes for potassium-ion batteries. *ACS Appl Energy Mater*. 2018;1:1828-1833.
99. Liu SL, Mao JF, Zhang Q, et al. An intrinsically non-flammable electrolyte for high-performance potassium batteries. *Angew Chem Int Ed*. 2020;59:3638-3644.
100. Zhang W, Wu Z, Zhang J, et al. Unraveling the effect of salt chemistry on long-durability high-phosphorus-concentration anode for potassium ion batteries. *Nano Energy*. 2018;53:967-974.
101. Zhang Q, Mao JF, Pang WK, et al. Boosting the potassium storage performance of alloy-based anode materials via electrolyte salt chemistry. *Adv Energy Mater*. 2018;8:1703288.
102. Xiao N, McCulloch WD, Wu Y. Reversible dendrite-free potassium plating and stripping electrochemistry for potassium secondary batteries. *J Am Chem Soc*. 2017;139:9475-9478.
103. Madec L, Gabaudan V, Gachot G, Stievano L, Monconduit L, Martinez H. Paving the way for K-ion batteries: role of electrolyte reactivity through the example of Sb-based electrodes. *ACS Appl Mater Interfaces*. 2018;10:34116-34122.
104. Cheng N, Zhao JG, Fan L, et al. Sb-MOFs derived Sb nanoparticles@porous carbon for high performance potassium-ion batteries anode. *Chem Commun*. 2019;55:12511-12514.
105. Gabaudan V, Touja J, Cot D, Flahaut E, Stievano L, Monconduit L. Double-walled carbon nanotubes, a performing additive to enhance capacity retention of antimony anode in potassium-ion batteries. *Electrochem Commun*. 2019; 105:106493.


## AUTHOR BIOGRAPHIES

**Hong Gao** received her PhD in material science at University of Wollongong, Australia in 2018. Currently, she is working as a postdoctoral research fellow at School of Environmental and Chemical Engineering, Shanghai University. Her research interests focus on energy storage materials for lithium-, sodium- and potassium-ion batteries.

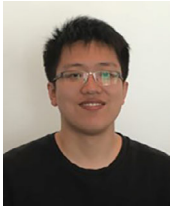

**Xin Guo** is currently working as a Research Fellow at Centre for Clean Energy Technology, University of Technology Sydney (UTS). He received his PhD degree from Faculty of Science at UTS in 2019. His research focuses on synthesis and applications of nanostructured functional materials, such as carbon-based composites, alloys, and 2D materials for energy storage and conversion.

**Hao Liu** is an ARC Future Fellow at University of Technology Sydney (UTS). He obtained PhD degree from University of Wollongong in 2011. He worked as a research associate in University of Queensland for one and half years and moved to UTS in 2012. Dr Liu interests in the synthesis of nanostructured materials and their applications in the fields of rechargeable batteries, supercapacitors, and electrocatalysts.

**Guoxiu Wang** is a Distinguished Professor and the Director of the Centre for Clean Energy Technology at University of Technology Sydney. He is an expert in materials chemistry, electrochemistry, energy storage and conversion, and battery technologies. His research interests include lithium-ion batteries, lithium-air batteries, sodium-ion batteries, lithium-sulfur batteries, supercapacitors, hydrogen, storage materials, fuel cells, electrocatalysis for hydrogen production, graphene, MXene, and other 2D functional materials for energy storage and conversion.

**How to cite this article:** Gao H, Guo X, Wang S, Zhang F, Liu H, Wang G. Antimony-based nanomaterials for high-performance potassium-ion batteries. *EcoMat*. 2020;2:e12027. https://doi.org/10.1002/eom2.12027